ResearchGate

See discussions, stats, and author profiles for this publication at: https://www.researchgate.net/publication/290796878

Biomechanics of bone: Applications for assessment of bone strength

Article · January 1985

CITATIONS
55

READS
603

2 authors, including:

Wilson C Hayes
Hayes + Associates, Inc.

335 PUBLICATIONS **24,637** CITATIONS

SEE PROFILE

All content following this page was uploaded by Wilson C Hayes on 13 June 2016.

The user has requested enhancement of the downloaded file.

Chapter 9

BIOMECHANICS OF BONE: APPLICATIONS FOR ASSESSMENT OF BONE STRENGTH[1]

W. C. Hayes and T.N. Gerhart

Orthopaedic Biomechanics Laboratory, Department of Orthopaedic Surgery, Charles A. Dana Research Institute, Beth Israel Hospital and Harvard Medical School, Boston, MA, U.S.A.

A. INTRODUCTION

Bone is the primary structural element of the human body. It serves to protect internal organs and allows the skeletal motions necessary for survival. Bone is also unique among structural materials in that it is self-repairing and can alter its properties and configuration in response to changes in mechanical demand (1,2). Bone density changes are commonly observed with aging, after periods of disuse, or as a result of chronic exercise (2-4). Changes in bone form are observed during fracture healing (5), with aging, and following certain operative procedures. Understanding these phenomena, which appear to be adaptive, stress-related events, has been a central focus of bone physiology for over a century.

Certain skeletal conditions such as osteoporosis can seriously compromise the structural integrity of the skeleton (3,6). The associated reduction in bone mass gradually increases vulnerability to fracture, particularly of the femoral neck and vertebrae (3,4,7). The frequency of osteoporosis in the United States is well recognized, with 50% of women 45 years of age or older exhibiting radiographic evidence of osteoporosis of the lumbar spine (7). Sixteen to 18 million women in the United States have a significant degree of vertebral atrophy and over 4 million people 50 years of age or older have osteoporosis severe enough to cause vertebral fractures. Epidemiologic studies suggest that from 15 to 30% of all white females in the United States develop symptomatic osteoporosis (4,7). Of the approximately 1 million fractures experienced each year by women 45 years of age or older in the United States, about 700,000 are incurred by women with osteoporosis.

Diagnostic tools for the differentiation and quantification of osteoporosis include determination of endocrine dysfunction, calcium balance, malabsorption, and liver and renal function. Perhaps the most important invasive method is the transiliac bone biopsy (8), a procedure which is widely recognized as reliable for indicating general skeletal disease. Histomorphometric analysis allows quantification of the amount of bone loss, classification of active and inactive surfaces, and identification of defects in bone mineralization (8).

Noninvasive techniques (9-12) for identifying bone loss include the use of radiographic features such as the Singh index of femoral trabecular pattern (13). Such indices appear to aid in identifying osteoporosis in general populations but exhibit only moderate correlations with bone density and fracture incidence. Radiographic morphometry (14) and radiographic photodensi-

---

1 We gratefully acknowledge the support of NIH AM 26740, AM 33066-01, RCDA AM 00749 and the Angus Foundation.

Bone and Mineral Research/3
William A. Peck, editor.
© Elsevier Science Publishers B.V., 1985.
ISBN 0 444 90347 x.
$0.85 per article per page (transactional system).
$0.20 per article per page (licensing system).

tometry (15) both involve quantitative measures of standardized skeletal sites. Their interpretation, however, may depend on bone geometric features which change with age (16-18) and for which population norms are not available. Single and dual-energy photon absorptiometry (11,19-21) are currently widely used since they are both accurate and highly reproducible. The degree of correlation with osteoporosis, however, depends on the anatomic site. Interpretation of the results must be made with care due to a sensitivity to changes in cross-sectional geometry. Other noninvasive techniques based on radionuclide uptake, Compton scattering, and neutron activation are still considered experimental or are not widely available. Computerized tomography (CT) for diagnostic imaging provides a new method for assessing skeletal mineral with a number of advantages over other available tehcniques (22-28). These include: 1) display of cross-sectional geometry with separation of trabecular and cortical bone; and 2) determination (in the dual energy mode) of bone mineral in the presence of unknown fat and soft tissue content.

Osteoporosis is clearly a serious national health problem which can be expected to increase along with the average age of the population. Despite advances in understanding its pathophysiology and major efforts to develop improved diagnostic tools, the identification of individual patients who are at increased risk of fracture remains an elusive goal. In fact, in many clinical settings, the occurrence of spontaneous vertebral fractures provides the only conclusive evidence of disease. Although such fractures are the major clinical sequelae of osteoporosis, the biomechanics of osteoporotic bone have received little attention. Thus, the structural consequences of known levels of bone loss are not well quantified.

These gaps in knowledge may be attributed to a general lack of interaction between the scientific disciplines associated with metabolic bone disease and those involved in orthopaedic biomechanics. For example, except in rare instances, the clinical procedures used in the diagnosis of osteoporosis (photon absorptiometry, CT) have been evaluated for accuracy only against other procedures which are themselves subject to significant measurement error (histomorphometry, neutron activation). On occasion, physical parameters such as ash weight or apparent density are employed but these are seldom related to the biomechanical characteristics of the measurement site or to the structural behavior of skeletal regions which exhibit high fracture risk. In light of the national health impact of osteoporosis (manifested primarily through increased rates of fracture) and the potential risk associated with many forms of therapy, reversal of this failure to focus on the biomechanical aspects of the disease represents a major challenge to investigators in the field.

The objective of this chapter is to provide an introduction to the mechanical behavior of bone as a material and of bones as living structures. This relationship between the mechanical behavior of bone tissue as a material and the structural behavior of whole bones suggests that we should approach the biomechanics of bone at two levels. At one level, we can perform standardized mechanical tests on uniform specimens of bone and determine the material properties of the tissue. We can also test the structural behavior of the whole bone (which represents an organized construct of bone tissues in a complex geometric arrangement). It is important to realize that bone fracture represents both failure of bone tissue at the material level and of the whole bone at the structural level. To predict the fracture behavior of bone tissue requires a critical analytical step involving calculation of the internal stresses in the whole bone. This step involves some knowledge of the geometric features of the whole bone and of the loads being applied.

Once the internal stresses are known, they can be compared to the known material properties of the bone tissue to provide an assessment of fracture risk.

We should also realize that the biological nature and metabolic activity of bone does not change, at least in the short term, the fact that bone is a structural material the function of which is to allow the various activities of daily living. As a structural material, bone is subject to the same engineering laws which govern the behavior of nonbiologic materials. This is a great convenience since it allows us, over the short term, to ignore many of the complex biological activities taking place in bone. This assumption does not hold over the long term, however, since changes in bone metabolism, disease and the normal aging process can result in important changes both in the material properties of bone tissue and in the structural and geometric features of whole bones. Under these conditions, the structural behavior of whole bones cannot then be expected to remain constant.

This chapter first provides some background material on basic concepts which can be used to describe the mechanical behavior of bone as a material and of bones as structures. No attempt is made to be comprehensive or particularly rigorous; the intent instead is to focus on a few simple biomechanical situations which illustrate the required concepts. After this introduction, some of the most important data on the material properties of cortical and trabecular bone are presented. Biomechanical examples, drawn primarily from areas related to metabolic bone disease, are then used to emphasize the practical applications of these concepts. Examples include measurements of geometric adaptation of bones with aging and their implications for photon absorptiometry, and some current attempts to predict vertebral fracture risk based on CT scans. It is our hope with this presentation to contribute to an improved dialogue between those interested in the biological and pathophysiological aspects of metabolic bone disease and those interested in the structural behavior of bone.

B. BASIC CONCEPTS

1. Material versus structural behavior

When forces are applied to any solid object, the object will be deformed from its original dimensions. At the same time, internal forces will be produced within the object. The deformations created at any point are referred to as the strains at that point. The internal force intensities (force/area) are referred to as the stresses at that point. When a bone is subjected to forces, these stresses and strains are introduced throughout the structure and can vary in a complex manner. To avoid some of these complexities and demonstrate some important mechanical concepts, it is useful to focus on a regular structure loaded (i.e., subjected to physical forces) under well-defined conditions (Figure 1). Similar specimens of regular geometry are used to determine the material properties of bone tissue. In Figure 1, a cylindrical bar of length L and a constant cross-sectional area (A) is shown subjected to pure tensile loading (F). As load is applied, the cylinder begins to stretch. This situation can be described by analogy to the stretching of a spring:

$$F = kx \qquad \text{Equation (1)}$$

where F is the applied force, x is the change in length of elongation of the spring, and k is the spring constant or stiffness of the spring. Inverting this simple relationship ($x = F/k$) demonstrates that with a very stiff spring

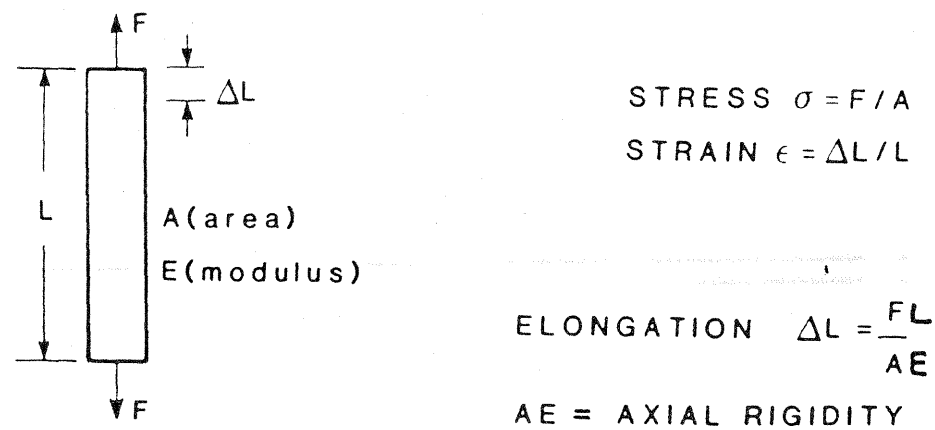

Figure 1. Tensile loading of a cylindrical rod of uniform cross-sectional geometry. The elongation is inversely proportional to the axial rigidity, AE.

high k), the elongation x is small for a given applied force. The analogous relation for stretching of the cylinder is:

$$\Delta L = FL/AE \qquad \text{Equation (2)}$$

where (ΔL) is the elongation of the cylinder, L is the original unstretched length, A is the cross-sectional area, F is the force, and E is the stiffness (or modulus) of the material. According to the simple relationship shown in Equation (2), the elongation (ΔL) is directly proportional to the applied force and to the original length and inversely proportional to the cross-sectional area and to the modulus of the material. Note particularly the combination of a geometric parameter (area, A) and a material parameter (modulus, E) in the denominator of this relationship. The combination AE occurs frequently and is referred to as the axial rigidity. Note also from Figure 1 that the total elongation depends both on the original length and on the cross-sectional area of the bar.

We can plot a force-deformation curve to represent the structural behavior of the cylindrical bar (Figure 2a). A cylinder of bone tested in tension would yield a linear region (also known as the elastic region) from 0-Y. At Y, "yielding" occurs and there is an internal rearrangement of the structure, often involving damage accumulation (29,30). In the region Y-U, non-elastic deformation occurs until finally, at U, fracture results in the loss of load-bearing capacity of the bar. It is particularly important to note that a force-deformation curve expresses the mechanical behavior of the structure since the curve would differ for a cylindrical bar of different cross-sectional area or different length (Equation 2).

To provide a standardized representation of the mechanical behavior of the material (as opposed to the behavior of the structure) we plot a normalized curve known as a stress-strain curve (Figure 2b). This normalizes the force-deformation relationship (i.e., eliminates the influence of the geometry

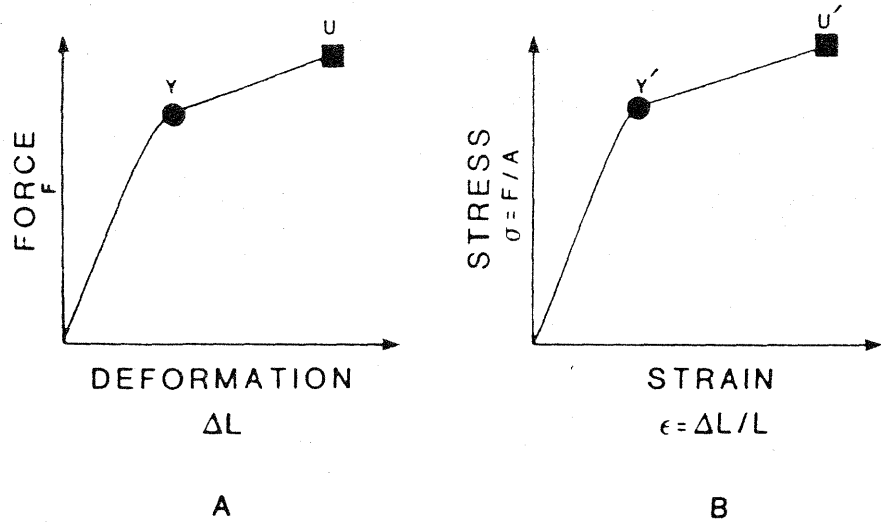

Figure 2. Material versus structural behavior: a) a force-deformation curve describes structural behavior since it reflects both geometric characteristics and material properties; b) a stress-strain curve describes material behavior since the influences of geometric characteristics have been eliminated by normalizing for the cross-sectional area and the original length.

of the cylinder) by dividing the applied force (F) by the cross-sectional area (A) and the deformation (ΔL) by the original length (L). We define this internal force intensity as stress (σ). The units of stress are Newtons/m^2 or Pascals (Pa). [1 Newton = 0.225 pounds force; 1 Pa = 6895 pounds per square inch (psi).] We often express stress in terms of megapascals (MPa) (1 MPa = 1×10^6 Pa), or gigapascals (GPa) (1 GPa = 1×10^9 Pa).

The ratio of the elongation to the original length is defined as the strain (ϵ). Note that strain is a non-dimensional quantity. In a stress-strain curve (Figure 2b), the slope of the linear elastic region is referred to as the modulus. Since the modulus is defined as the slope of the stress-strain curve in the elastic region and since the units of stress are MPa and strain is non-dimensional, the units of modulus are the same as those of stress, MPa or GPa. In the stress-strain curve at Y', the material yields at a stress level known as the yield strength (again with units of MPa). At U' the material fractures at a stress level known as the fracture strength or ultimate tensile strength (units of MPa). Note that the stress-strain representation allows us to compare different materials, both in terms of the slope of the stress-strain curve and these strength parameters. From such stress-strain curves, the modulus of steel is shown to be approximately 10 times that of cortical bone. The ultimate tensile strength of steel is approximately five times that of cortical bone.

2. Loading pattern in whole bones

Bones of the appendicular skeleton are long, slender, slightly curved elements which are loaded primarily by compressive forces applied at the joints. Because of this gentle curvature, bones are subjected to a combina-

tion of axial compressive forces and bending forces. It is therefore instructive to focus first on these two loading cases separately and then to examine how these load cases can combine to produce the general loading patterns of whole bones. We have already discussed the axial loading case for tension (Figure 1). Compressive loading is analogous except that the deformation L is now a shortening of the bar. The magnitude of this shortening is still given by L = FL/AE with the associated compressive stress being given by F/A. Recall that we refer to AE as the axial rigidity. By convention, compressive stresses are assumed to be negative, and tensile stresses are positive.

Fig 3

In engineering, long slender structures which are designed to resist transverse or bending loads are referred to as beams. Examples are the I-beams commonly used in civil engineering structures. Such beams are usually long in comparison to their cross-sectional dimensions and, for this reason, are similar to the long bones of the appendicular skeleton. A beam can be subjected to bending loads by applying two sets of forces near the beam ends (Figure 3). To make this loading situation clearer, imagine grasping a yardstick near its ends in such a way that it is flexed into a bowed shape. The deflection of the mid-point of the beam is a relatively complex relationship involving the geometric characteristics of the beam and the location of the applied forces (as expressed by L and a), the magnitude of applied forces, the modulus of the beam material (i.e., as above, its stiffness), and a new quan-

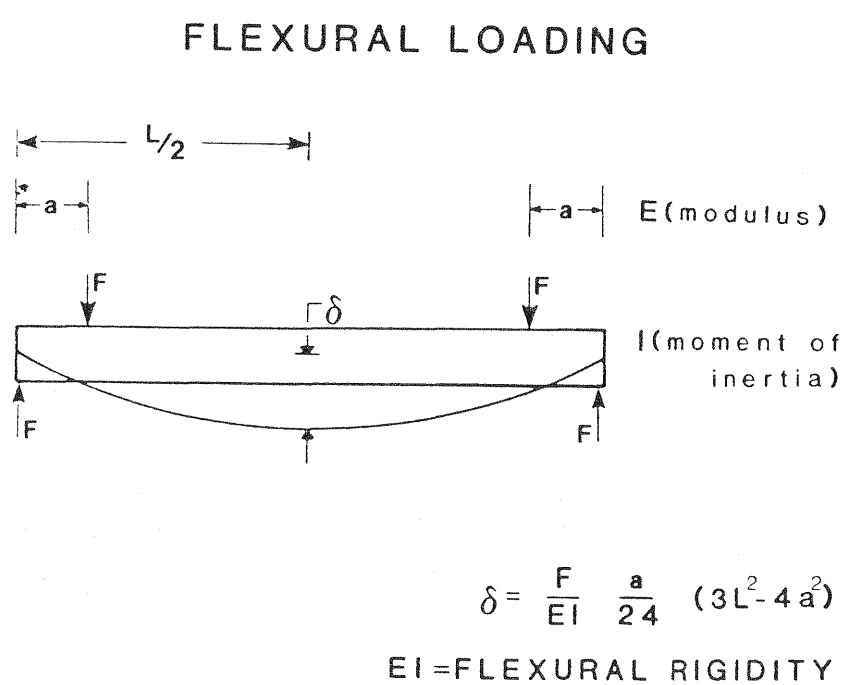

Figure 3. Flexural (bending) loading of a beam. The mid-span deflection is inversely proportional to the flexural rigidity, EI.

tity known as the moment of inertia. This geometric parameter expresses the characteristics of the distribution of the beam cross-sectional area in relation to a transverse axis. It reflects, for instance, the large differences in bending resistance of the yardstick bent when it is held flat versus when it is held on edge. We will return below to a further discussion of this geometric parameter. Note, however, that there are similarities between the expressions used to characterize axial loading and flexural loadings (Figures I and 3). In both cases, the deformations are directly proportional to the applied forces and to certain geometric features of the structure. In both cases, the deformations are inversely proportional to a combination of parameters reflecting material stiffness E and a geometric feature of the cross-section. In axial loading, we called this combination AE the axial rigidity. In bending (or flexure) we call this combination EI, the flexural rigidity.

To visualize the internal forces or stresses which occur in a beam, imagine holding the ends of the yardstick and bending it so as to produce a convex surface on one side and a concave surface on the other side. It can be shown that the material on the convex side of the beam is subjected to tensile (or stretching) strains. The material on the concave side will be subjected to compressive strains. This suggests that at some point between the two surfaces, the strains are zero (i.e., the original length of the beam is unchanged). This location is referred to as the neutral axis. The strains produced at any cross-section of the beam also result in stresses at that cross-section. The concave side of the beam is subjected to compressive stresses while the convex side experiences tensile stresses (Figure 4). Notice that the maximum stresses are experienced by the material on the surface of the beam. If the bending forces are increased until the bar begins to fracture, the fracture will be initiated at the surface of the beam where the stresses are highest.

Because bones are slightly curved and are subjected to compressive loads applied at the joint surfaces, the most common loading situation in vivo is a combination of compressive and bending loads. The resulting stresses on a transverse section through a slightly curved member can be found by summing the stresses caused by the compressive axial forces and by the bending stresses (Figure 5). As a result of the addition of the compressive stresses from axial loading and the compressive stresses from bending, even higher compressive stresses will be created on the concave side of the bar, while the convex side will experience either reduced compressive stresses or even tensile stresses, depending on the magnitude of the axial force and its eccentricity. These stresses can be described with reasonable accuracy by simply combining the stresses due to axial compression with those from bending:

(combined stress) = (compressive stress) $\pm$ (bending stress).

Or, in mathematical terms, this can be written

$$\sigma_{max} = \frac{P}{A} \pm \frac{ePc}{I} \qquad \text{Equation (3)}$$

where P is applied load, e is its eccentricity (the distance from the neutral axis to the line of action of the force), and c is the distance from the neutral axis to the convex and concave surfaces of the beam. The parameter I (defined below) is again the moment of inertia of the cross-section and reflects the shape and distribution of the cross-sectional area.

Equation (3) may be easily adapted to define the maximum tensile stress, which occurs on the convex surface:

$$\sigma_t = -\frac{P}{A} + \frac{ePc}{I} \qquad \text{Equation (4)}$$

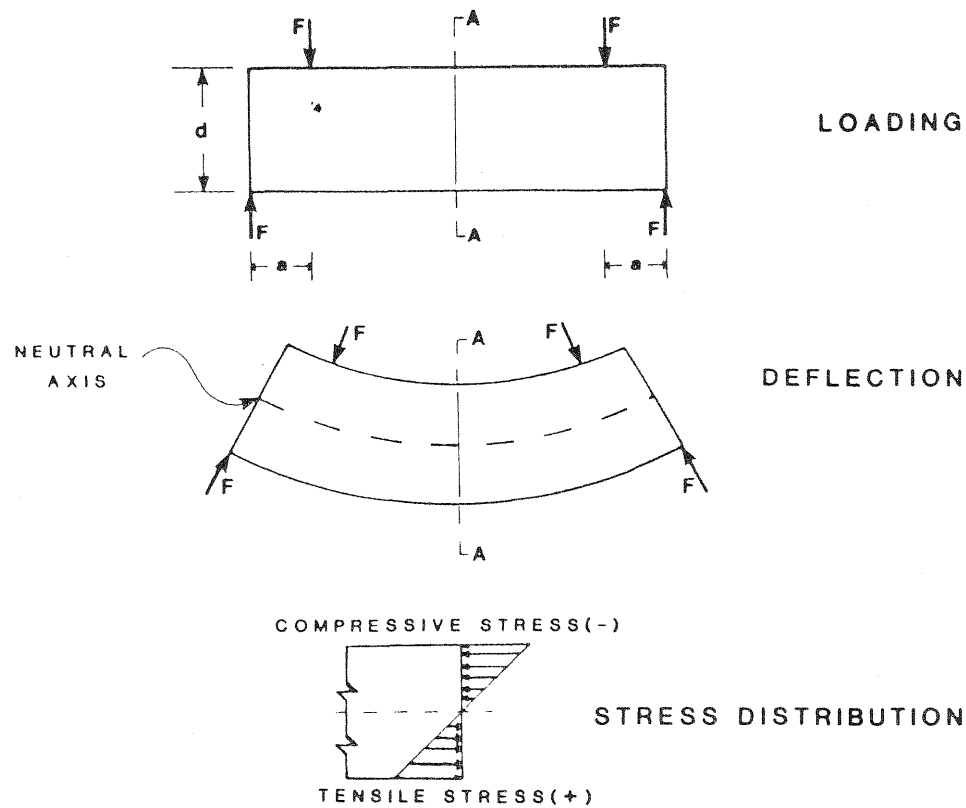

Figure 4. Stresses associated with flexural loading of beams. Tensile stresses are generated on the convex surface and compressive stresses on the concave surface. The unstressed central region is referred to as the neutral axis.

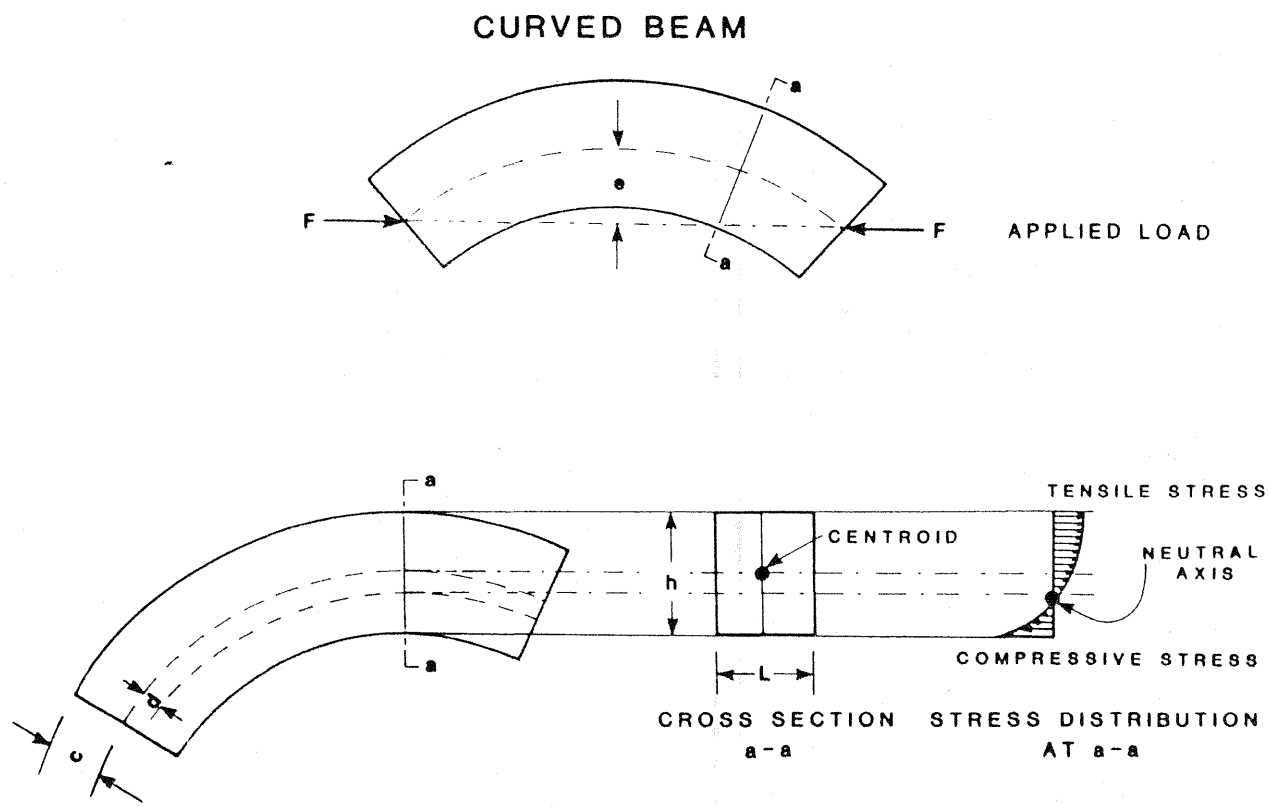

Figure 5. Stresses due to eccentric axial compressive loading of a slightly curved beam. Due to the eccentricity of the applied load, stresses due to axial compression and bending are combined, resulting in reduced tensile stresses on the convex surface and increased compressive stresses on the concave surface.

The maximum compressive stress, which occurs on the concave surface, may also be defined:

$$\sigma_c = -\frac{P}{A} - \frac{ePc}{I} \qquad \text{Equation (5)}$$

Note particularly that the compressive stresses from axial loading and bending are of the same sign (additive) while the two contributions to stresses on the tensile surface are of opposite sign (Figure 5). Also, these relationships for the stresses in a curved beam reflect a number of geometric features of the loading and of the beam. Such features include both the cross-sectional area and the moment of inertia, the eccentricity of the applied load, and the distance from the neutral axis to the convex and concave surfaces of the beam. Similar situations occur in long bones and, in general, compressive stresses are higher than the tensile stresses throughout the appendicular skeleton.

3. Geometric features of long bones

The above discussion of loading patterns suggests that there are several aspects of bone cross-sectional geometry that are important to the structural behavior of whole bones. These include the cross-sectional area (A) and the moment of inertia (I). The area of course reflects the size of the bone cross-section. Subjected to axial compressive loads, a large bone is more resistant to fracture [Equation (2)] simply because it distributes the internal forces over a larger surface area (resulting in lower stresses).

The moment of inertia expresses the shape of the cross-section and the particular distribution of the cross-sectional area with respect to the applied bending loads. This statement is important since it suggests that the moment of inertia must always be expressed with relation to a particular axis. Expressions for the moments of inertia for several regular geometric cross-sections (calculated with respect to a transverse axis through the centroid or center of the area) are shown in Figure 6. Methods for calculating moments of inertia can be found in any calculus text. Such calculations are equivalent to dividing the cross-sectional area into small elemental areas, multiplying each area element by the square of its distance to the axis of interest, and then summing over all elements. Thus, the moment of inertia is highly sensitive to the distribution of area with respect to the axis. An area that is at a greater distance from the neutral axis (i.e., the unstretched axis of the beam) is much more efficient in resisting bending with respect to that axis. These concepts demonstrate why a yardstick turned on edge resists bending more efficiently than a yardstick turned horizontally. (Verify this using the relationship shown in Figure 6). The influence of moments of inertia also explains why an I-beam (Figure 6) is such an efficient section for resisting bending in one direction, since most of the material is located at distance from the neutral axis.

If bones were subjected to bending loads in only one direction, their cross-sectional shapes would probably have evolved toward something like an I-beam. Instead, long bones are loaded, as suggested above, by axial compression, bending (in multiple directions), and torsion. Under these conditions, the most efficient cross-sectional shape is the cylindrical tube. A tubular structure can better distribute the stresses imposed by bending and torsional loading than can a solid bar of the same cross-sectional area, since the material is distributed at a greater distance from the central axis. Figure 7 shows three cylindrical rods of different cross-sectional geometries. Bar A is a solid cylinder and has a radius of .94 cm. Bar B is a hollow tube of outer radius 1.09 cm and inner radius .53 cm. Note that the areas of A and B

CROSS-SECTION	MOMENT OF INERTIA
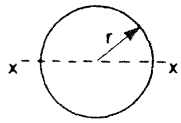	$I_{xx} = \pi r^4/4$
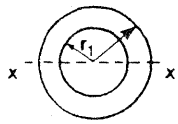	$I_{xx} = \pi(r_0^4 - r_1^4)/4$
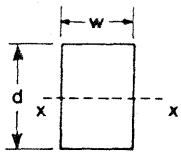	$I_{xx} = wd^3/12$
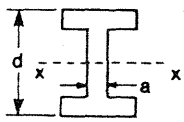	$I_{xx} = \frac{wd^3 - (w-a)(d-2a)^3}{12}$

Figure 6. Moments of inertia for some common structural cross-sections.

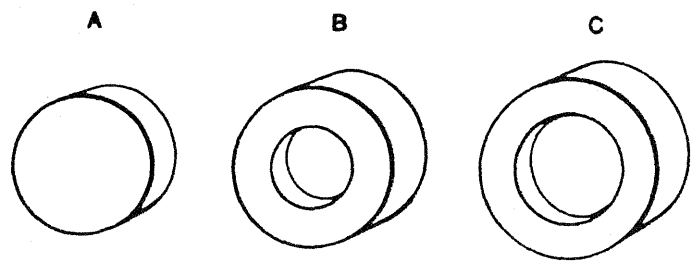

	A	B	C
AREA (cm^2)	2.77	2.77	2.84
MOMENT OF INERTIA(cm^4)	.61	1.06	1.54
BENDING STRENGTH(%)	100%	149%	193%

Figure 7. Effects of changes in distribution of cross-sectional area on the area, moments of inertia and bending strength of some regular cylindrical geometries. These idealized geometries reflect the approximate dimensions of the femoral mid-shaft in the Pecos Pueblo population (16). The changes between B and C are thus comparable to the geometric remodeling that occurred with aging in that population.

are approximately the same. Bar C is again a hollow tube, but in this instance both the outer radius and the inner radius have been increased by 1.25 cm and .76 cm, respectively. The values for the cross-sectional areas and moments of inertia of these simple shapes are also shown in Figure 7. Since the tensile or compressive strengths are inversely proportional to the cross-sectional area ($\sigma = -F/A$), bars A and B exhibit similar strengths and bar C is increased in strength by about 3%. In bending loading, however, the more favorable distribution of the cross-sectional area results in increases in bending strengths by factors of 1.49 and 1.93 for bars B and C. In particular, the changes in inner and outer radii for tube C in comparison to B result in an increase in bending strength by a factor of about 1.29. These idealized cross-sectional geometries are based on the approximate dimensions of the human femoral mid-shaft in an archaeological sample (16,17,31) and approximate the change in cross-sectional properties with age in that sample. The consequences of these age-related geometric changes for fracture of the femoral shaft are addressed below.

Of course, bone cross-sectional geometries are not as regular as the simple geometric shapes discussed above. In order to describe as accurately as possible the structural behavior of whole bones and to provide increased precision in describing the effects of age, gender, cultural factors, and exercise, we have developed computer software which provides automated calculation of all the necessary geometric parameters (32). The method requires that periosteal and endosteal boundaries of the cross-section be traced on a digitizer and then provides values for area, centroid location and the moments of inertia. These methods have been used to characterize bone geometry changes with age in both modern and archaeological populations (16,17,31). The results will also be discussed below.

C. MECHANICAL PROPERTIES OF BONE TISSUE

1. Material properties of cortical bone

The fracture behavior of whole bones is strongly dependent upon the material behavior of the bone tissues. To determine the mechanical properties of bone tissue we test small, uniform specimens which are loaded under well-defined conditions. Such testing conditions produce uniform, known stresses throughout the specimen (Figure 1). Specimen deformation can then be measured and the strains calculated using the relationships we have described. The material properties of the tissue can thus be determined for the specific loading conditions imposed. This general approach to materials testing has allowed documentation of cortical bone material properties in tension, compression, bending, and torsion (29,30,33-42).

Several factors influence the material properties of cortical bone. One factor is the rate at which the bone tissue is loaded. A specimen of cortical bone which is very rapidly subjected to forces will have a greater elastic modulus and ultimate strength than bone tissue which is loaded more slowly. In addition, bone tissue which is loaded very rapidly absorbs considerably more energy than bone tissue which is loaded more slowly. To quantify the rate of deformation, one can refer to the strain rate (units = sec^{-1}) to which the tissue is exposed during the loading process. In normal activities, bone is subjected to strain rates that are generally below 0.01 sec^{-1}. Materials such as bone for which stress-strain characteristics and strength properties depend upon the applied strain rate are said to be visco-elastic (or time-dependent materials). However, this rate dependency is relatively weak (41). The elastic modulus and ultimate strength of bone are

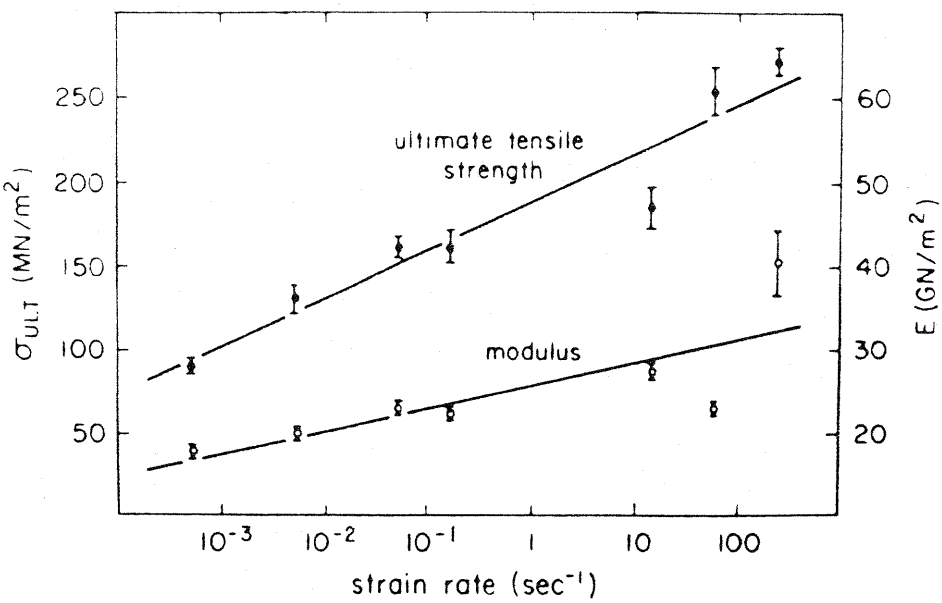

Figure 8. The influence of loading rate on the tensile strength and modulus of cortical bone (41). The ultimate tensile strength increases by about a factor of 3 and the modulus by a factor of 2. From Wright and Hayes (41); used with permission.

approximately proportional to the strain rate raised to the 0.06 power (Figure 8). Thus, over a very wide range of strain rates, the ultimate tensile strength increases by a factor of three and the modulus increases by about a factor of two.

The stress-strain behavior of cortical bone is also strongly dependent upon the orientation of the bone microstructure with respect to the direction of loading. Several investigators have demonstrated that cortical bone is stronger and stiffer in the longitudinal direction (direction of osteon orientation) than in the transverse direction. In addition, bone specimens loaded in a direction perpendicular to the osteons tend to fail in a more brittle manner, with little nonelastic deformation after yielding. Long bones are therefore better able to resist stresses along the axis of the bone than across the bone axis. Material such as bone for which elastic and strength properties are dependent upon the direction of applied loading are said to be anisotropic materials. The viscoelastic and anisotropic nature of cortical bone distinguish it as a complex material. Because of these characteristics, one must specify the strain rate and the direction of applied loading when describing material behavior.

Ultimate strengths of adult femoral cortical bone under various modes of loading in both longitudinal and transverse directions (29,30,43) are summarized in Table 1. These results indicate that the material strength of bone tissue depends upon the type of loading as well as on the loading direction. The compressive strength is greater than the tensile strength in both longitudinal and transverse directions. Transverse specimens are weaker than longitudinal specimens in both tension and compression. The shear properties

Table 1. Strength of femoral cortical bone.*

Loading Mode	Ultimate Strength (MPa)
Longitudinal	
Tension	133
Compression	193
Shear	68
Transverse	
Tension	51
Compression	133

* Mean values from Reilly and Burstein (53). Age span of population, 19-80 years.

Table 2. Modulus of femoral cortical bone.*

Longitudinal	17.0 GPa
Transverse	11.5 GPa
Shear	3.3 GPa

* Mean values from Reilly and Burstein (53). Age span of population, 19-80 years. 1 GPa (gigapascal) = 1000 MPa.

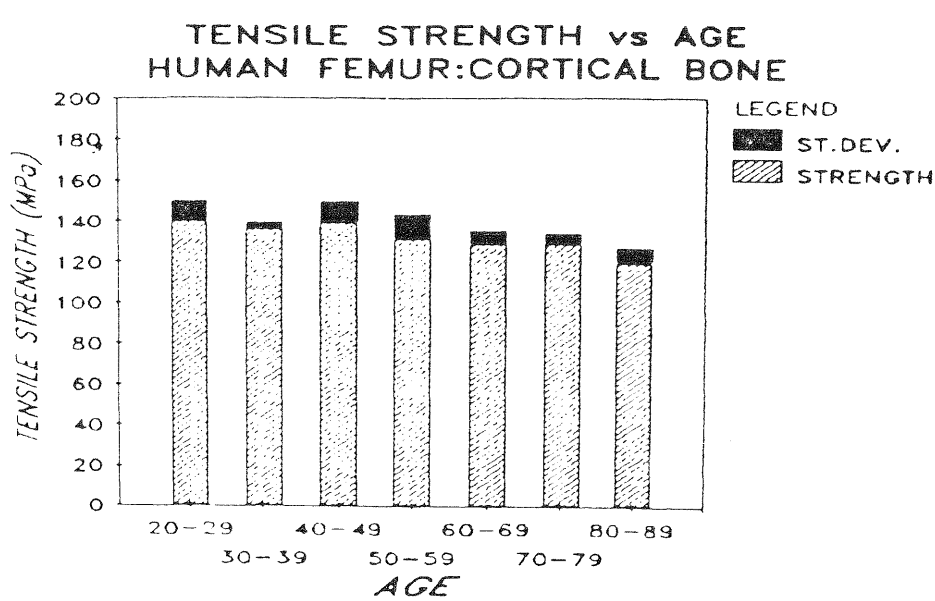

Figure 9. Reductions with age in the tensile strength of human cortical bone from the femoral diaphysis (36). Strength changes of about 2% per decade are observed.

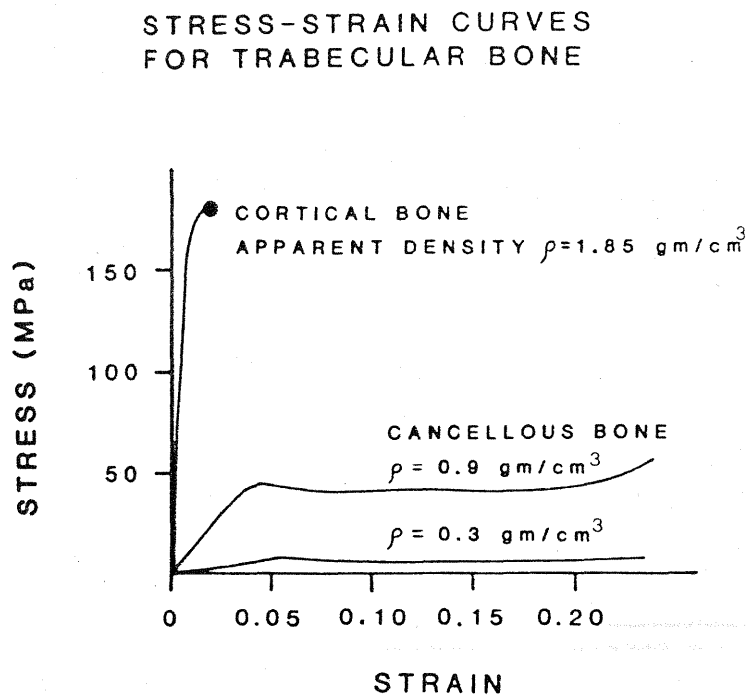

Figure 10. Typical stress-strain curves for trabecular bone of different apparent densities.

(determined by torsion tests about the longitudinal axis and reflecting shear stresses along transverse and longitudinal planes) are about one-third of the compressive strength. The modulus values for adult femoral cortical bone are shown in Table 2 (29,30,43). The longitudinal elastic modulus is about 50% greater than the transverse elastic modulus. The shear modulus for torsion about the longitudinal axis is about one-fifth the longitudinal modulus.

The material properties of cortical bone also decline with age (36) (Figure 9). Both tensile strength and modulus decrease about 2% per decade over the age range 20-90. Thus, the ultimate tensile strength declines from 140 MPa in the third decade to 120 MPa in the ninth decade. Over the same period, the elastic modulus decreases from 17 GPa to 15.6 GPa (36).

2. Material properties of trabecular bone

The major physical difference between trabecular bone and cortical bone is the higher degree of porosity exhibited by trabecular bone. This porosity is reflected by measurements of the apparent density (i.e., the mass of bone tissue divided by the bulk volume of the test specimen, including mineralized bone and bone marrow spaces). In the human skeleton, the apparent density of trabecular bone ranges from approximately 0.1 g/cm^3 to 1.0 g/cm^3. The apparent density of cortical bone is about 1.8 g/cm^3. A specimen with an apparent density of 0.2 g/cm^3 has a porosity of approximately 90%.

Bone apparent density has a profound influence on the compressive stress-strain behavior of trabecular bone (44,45) (Figure 10). These stress-

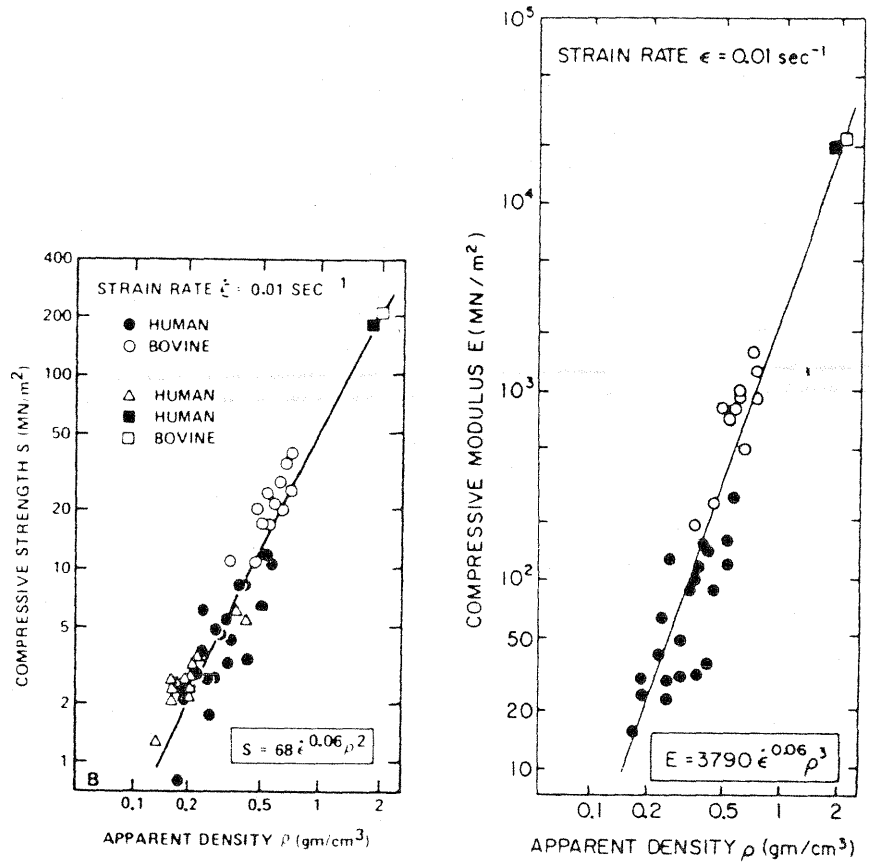

Figure 11. Influence of apparent density on the compressive strength and modulus of trabecular bone. Filled circles represent human trabecular bone tested in compression. Empty circles and empty traingles represent bovine and human trabecular specimens tested in compression at strains of 0.01 and 0.1/sec, respectively. Filled and empty squares represent human and bovine compact bone, respectively. From Carter and Hayes (45); used with permission.

strain properties are markedly different from those of cortical bone and are similar to the compressive behavior of many porous engineering materials which can be used to absorb energy on impact. The stress-strain curve for trabecular bone exhibits an initial elastic region followed by yield. Yielding occurs as the trabeculae begin to fracture. Yield is then followed by a long plateau region which is created as progressively more and more trabeculae fracture. The fractured trabeculae begin to fill the marrow spaces and, at a strain of approximately 0.50, most of the marrow spaces have filled with the debris of fractured trabeculae. Further loading of trabecular bone after pore closure is associated with a marked increase in specimen modulus.

Both the compressive strength and the compressive modulus of trabecular bone are markedly influenced by the apparent density of the tissue (Figure 11). The regressions presented in Figure 11 include cortical bone

with an apparent density of approximately 1.8 g/cm^3 as well as trabecular bone specimens representing a wide range of apparent densities. These relationships indicate that the compressive strength of all bone tissue in the skeleton is approximately proportional to the square of the apparent density (44,45). The elastic modulus of all bone tissue is approximately proportional to the cube of the apparent density. Although these relationships were initially derived from compression tests, tensile tests of trabecular bone indicate that its strength in tension is approximately the same as that in compression (46). In addition, the elastic modulus of trabecular bone is approximately the same in both tensile and compressive loading.

These relationships between mechanical properties and the apparent density of bone tissue are of profound physiological and biomechanical importance. First, they indicate that bone tissue can generate large changes in modulus and strength through small changes in bone apparent density. Conversely, subtle changes in bone apparent density result in large differences in strength and modulus. This is a sobering thought if we recall that bone density changes are usually not evident radiographically until the bone density has been reduced by 30-50%. The power-law relationships shown in Figure 11 indicate that such reductions in bone density result in nearly an order of magnitude reduction in bone stiffness and strength.

3. Material properties of the metaphyseal shell

The structural contributions of the thin metaphyseal shell represent a major uncertainty in understanding increases in fracture risk associated with osteoporosis. In almost all previous studies of metaphyseal regions, material property values for these regions have been assumed to be close to the values for diaphyseal cortical bone described above. In addition, shell thicknesses ranging from 0.5 to 2.0 mm have been assumed in most previous studies of the structural behavior of metaphyseal region. Consequently, most workers have concluded that the metaphyseal shell plays a major structural role in joint loading and in the resistance of vertebral bodies to fracture. To provide direct measurements of the mechanical properties of the metaphyseal shell, we conducted experiments on small specimens removed from the proximal tibial metaphysis.

Proximal tibiae were harvested from fresh cadavers (age 59-90, mean age 74) and small (9.5 mm) plugs containing the shell and underlying trabecular bone were removed. Trabecular bone was carefully ground away to produce a thin disk of constant thickness. Specimens were prepared from: 1) proximal metaphysis (0-3 cm distal from tibial plateau); 2) distal metaphysis (3-5 cm) and 3) the proximal diaphysis (5-10 cm). Specimens were tested as simply supported, centrally loaded, circular plates and the modulus, yield strength and ultimate strength were determined using plate theory. The validity of the method was assessed using thin aluminum disks of similar geometry.

The values for yield strength and modulus of the metaphyseal shell for these regions are shown in Table 3. These values indicate that the modulus and yield strengths in the metaphyseal regions are far less than has been previously assumed. In the most proximal region, the yield strength (Table 3) is less than half the tensile strength of diaphyseal cortical bone (Table 1). The modulus is about one-tenth the modulus value for cortical bone of the shaft. Our modulus values of 7.05 ± 0.87 GPa in the proximal diaphysis are lower than the reported longitudinal values for cortical bone, but in good agreement with data for the circumferential direction.

Table 3. Mechanical properties of metaphyseal shell of the proximal tibia.

Distance from Tibial Plateau (cm)	Elastic Modulus GPa	Yield Strength GPa
0-3	1.43 (.46)	58.1 (32.9)
3-5	5.04 (.98)	105.0 (18.2)
5-10	7.05 (.87)	121.0 (13.1)

* Mean values (and 95% confidence intervals) from Murray et al (54).

These data indicate that previously assumed modulus values for the metaphyseal shell are high by a factor of from 10 to 20, and suggest that the axial rigidity of the metaphyseal shell may be more than an order of magnitude less than has been assumed. These findings have strong significance for the structural contributions of these regions, as we shall see below in a study of failure characteristics of lumbar vertebrae.

D. STRUCTURAL BEHAVIOR OF WHOLE BONE

When the skeleton is exposed to trauma, regions of it are subjected to very great forces. Fracture occurs when the local stresses exceed the ultimate strength of the bone in that region. Bone fracture can therefore be viewed as an event which is initiated at the material level and then affects the load-bearing capacity of the bone at the structural level. As indicated previously, the major difference between behavior at the material level and at the structural level relates to the inclusion of geometric features at the structural level and their exclusion at the material level. Thus, structural behavior includes both the effects of bone geometry and material properties, whereas material behavior basically occurs without the effects of complex bone geometries and involves only specimens of simplified geometry. Any attempt to predict the structural behavior of a skeletal region must therefore reflect both the heterogeneous material properties of the region and the complex geometric arrangement of each type of bone. To focus on this level of behavior and to address the structural consequences of changes in bone geometries and material properties with age, two studies are summarized. The first describes changes in the geometric features of long bones with age. In particular, we assess the consequences of these geometric changes for increased fracture risk and for the use of photon absorptiometry as a noninvasive procedure for determining bone mineral content. The second study involves the use of computed tomography as a noninvasive predictor of fracture risk in vertebral bodies of the lumbar spine.

1. Age-related changes in cross-sectional geometry of the lower limb

Age changes in bone mineral mass, volume and density in the human skeleton have been the subject of intensive investigation over the past 25 years. Changes with age in the histological and mechanical properties of bone have also been studied by many investigators. The general picture to emerge from these studies is a progressive net loss of bone mass with aging, beginning in the fifth decade and proceeding at a faster rate among women. Concurrent with this overall loss of bone is the change in bone material properties (36), resulting in bone tissue of reduced strength and modulus as described above. The major clinical consequence of these skeletal changes is an age-related increase in fracture incidence.

One structural variable which is not often considered in studies of skeletal aging is the global geometry of cortical bone. However, the

geometrical distribution of bone tissue, together with its material properties, is critical in determining the structural strength and rigidity of the whole bone. The results of radiogrammetric studies suggest that some geometric remodeling of long bone cortices occurs with aging. In particular, subperiosteal apposition of bone has been observed to occur concurrently with endosteal absorption. This remodeling of the diaphysis to a larger diameter may serve a mechanical "compensatory" function by increasing the moment of inertia as the cortex thins with aging.

An additional motivation for obtaining improved data on long bone cross-sectional geometry is to achieve normalization of photon absorptiometric measurements. Since its initial description, photon absorptiometry has become one of the most widely used techniques for assessing bone mineral content (BMC) of the skeleton in vivo (11,15). Many investigators have demonstrated an inverse relationship between BMC, or BMC divided by scan width (BW), usually measured in the radius, and previous or subsequent fracture incidence. While significant differences in mean BMC values in fracture and non-fracture groups have been demonstrated, these studies invariably also indicate a large overlap in values between the two groups. Thus, photon absorptiometry appears to be of limited value in distinguishing on an individual basis between high and low fracture risk patients. One reason for this difficulty may be the inherent limitations and assumptions involved in photon absorptiometry. BMC provides a summative mineral content across an entire bone scan path. As such, it is appropriate for monitoring sequential changes in total bone mineral at the scan site in individual patients. In order to compare BMC values in different individuals, however, some kind of "skeletal size" standardization must be carried out. Although several more sophisticated techniques have been proposed, the most common size standardization procedure has been simply to divide BMC by total (subperiosteal) bone width across the scan path. Nevertheless, the accuracy of bone width correcting for true bone volume has not yet been tested and several studies have suggested that BW is inadequate for use in normalizing BMC measurements for size, sex, or age differences. A second issue concerns variation in cross-sectional geometry at different longitudinal positions in the same bone. Finally, and perhaps most important, is the assumption that the geometry of the same scan site does not vary systematically by age, gender, or other variables related to bone metabolism.

We have previously reported cross-sectional geometric data on femora and tibiae from an archaeological sample of 119 individuals from the American Southwest (16,18). We showed increases with aging in both subperiosteal dimensions and in areal moments of inertia. We also documented significant differences between cross-sectional sites and between sexes in the pattern of cortical remodeling with age. Recently, we also addressed certain relationships between bone cross-sectional geometry and photon absorptiometric parameters for 11 femoral and tibial sites in the same population (31). The data showed that locational, age and sex differences in BMC are largely determined by variations in cortical area. In addition, because of differences in bone geometry, variations in bone width do not reflect variations in cortical area. As a consequence, use of BW to standardize for volumetric or bone "size" differences produces misleading results in sex and age comparisons. These results are briefly summarized here in order to suggest the changes in cortical cross-sectional geometry that can occur with age and to indicate some of the difficulties involved in using bone width as a normalization parameter for photon absorptiometric studies.

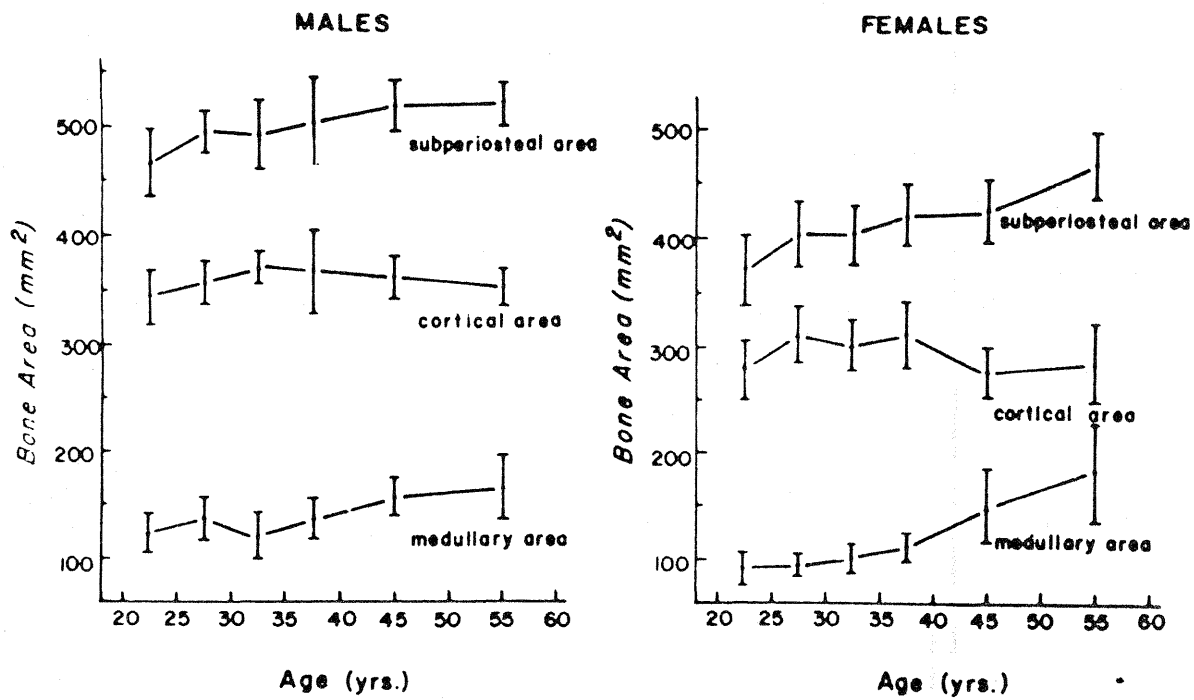

Figure 12. Changes with age in bone areas of the femoral mid-shaft for the Pecos Pueblo population. From (16); used with permission. Copyright 1982 by the American. Assn. Advancmt. Science.

a) Geometric compensation for age-related changes in long bones

A sample of femora and tibiae from 119 individuals was selected from the Pecos Pueblo archaelogical collections excavated from the large late prehistoric and protohistoric site in New Mexico (16,18). Pelvic and cranial morphology were used to determine sex, and age estimates were based upon pubic symphyseal form, functional dental wear, and endocranial suture closure. Each femur or tibia was sectioned perpendicular to its longitudinal axis at five diaphyseal sites corresponding to 20, 35, 50, 65 and 80% of the bone length, measured from the distal end. In addition, one side was sectioned to the femoral neck at its minimum superior-inferior breadth. Photographs of the cut and cross-sectional surfaces were rear-projected onto an electronic digitizer and subperiosteal and endosteal parameters were manually traced. Parameter point coordinates at 1 mm intervals were input into program SLICE (32) and geometric section properties (areas, moments of inertia and their orientation) were calculated.

Changes with age and bone areas of the representative cross-section—the femoral midshaft—are shown in Figure 12. In both sexes the area of the medullary (marrow) cavity and the total area bounded by the subperiosteal (outer) bone surface increase with age. However, although increases in total subperiosteal area are fairly similar in males and females (averaging 7% in males and 11% in females over all cross-sections), percentage increases in medullary area are much greater in females (39% versus 19% for males over all sections). Thus, because of relatively greater endosteal resorption of bone with aging, females show a significant decline in compact cortical bone area (average 10%), whereas males show only a negligible (1%) average decrease in cortical bone area.

Figure 13 illustrates the changes with age of the femoral midshaft in the maximum moment of inertia (I_{max}). For both sexes, despite age-related

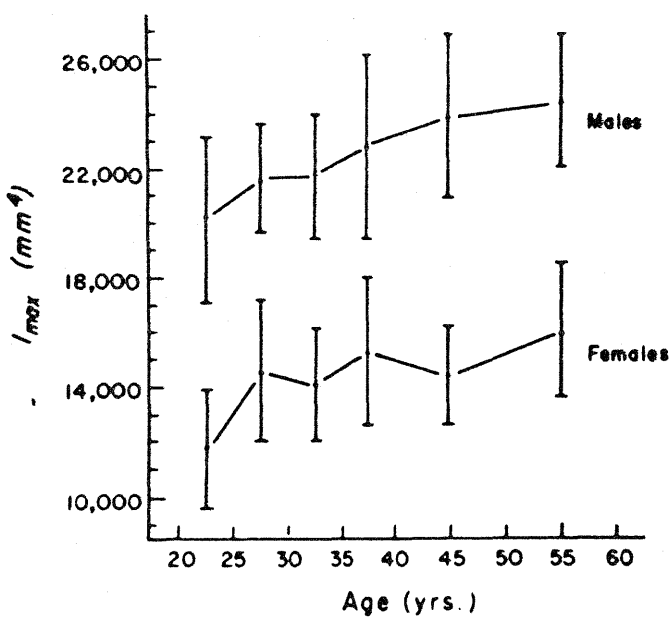

Figure 13. Changes with age in the maximum moment of inertia of the femoral mid-shaft for the Pecos Pueblo population. From (16); used with permission. Copyright 1982 by the American. Assn. Advancmt. Science.

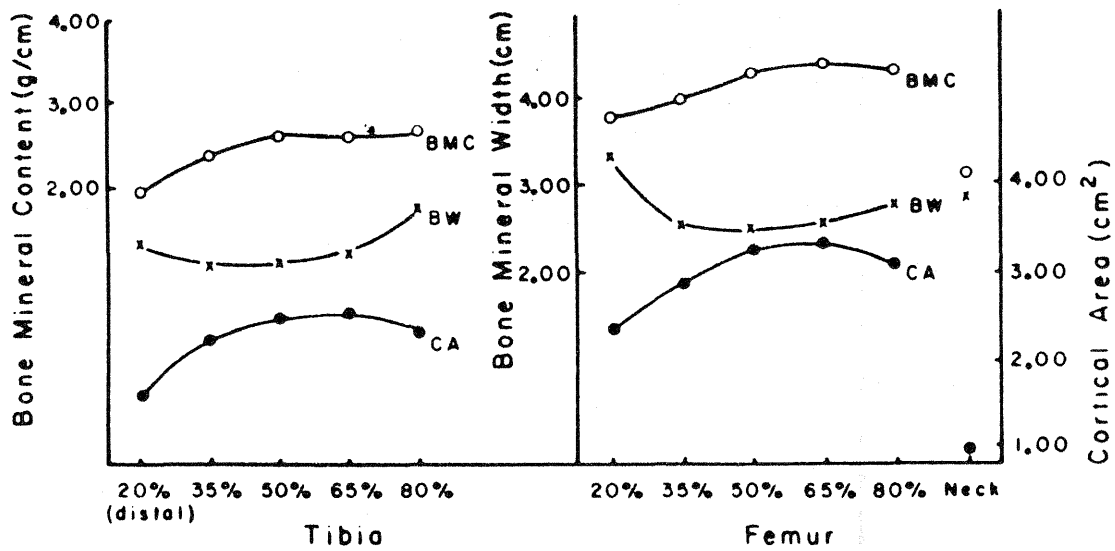

Figure 14. Patterns of variation in bone mineral content (BMC), bone width (BW), and cortical area (CA) at eleven cross-sectional sites for the Pecos Pueblo population. BMC and CA follow similar patterns whereas BW does not adequately reflect variations in CA. From (31); used with permission.

declines in cortical bone area, moments of inertia in femoral and tibial cross-sections increase. This is due to subperiosteal expansion and progressive remodeling into a cortex of larger diameter. With more bone placed farther from the section centroid, the cross-section is more efficient for resisting bending and torsion. These geometric changes have consequences for properly interpreting photon absorptiometric scans and for accurately assessing fracture risk in the appendicular skeleton.

b) Consequences for photon-absorptiometry

Photon absorptiometric scans were carried out at 11 cross-section locations in this same archaelogical sample using a Norland Cameron[I] Bone Mineral Analyzer with a 3.0 mm scan beam at a scanner speed of 2 mm/sec (31). Whole bones were submerged in 6 cm of water in a plexiglass box marked with reference axes and scanned twice at each site with the average BMC and BW (bone width) recorded. Scans at two of the cross-section locations—the femoral midshaft and the femoral neck—were taken on all 119 individuals included in the study sample.

The variations in BMC, BW, and CA (cortical area) at the 11 femoral and tibial cross-section locations are shown in Figure 14. Both BMC and CA follow quite similar patterns of longitudinal variation in the lower limb. In both the tibia and femur, BMC and CA increase from the most distal diaphyseal section to a peak in the proximal half of the diaphysis. The only significant departures from parallelism between the two curves occur in the most proximal and distal sections where CA tends to decline more than BMC. By contrast, BW and CA do not follow similar patterns of longitudinal variation in the lower limb. Moreover, the pattern of variation in BW is almost diametrically opposite that of CA or BMC, reaching minimum value at or near the locations of peak values in the other two properties. These differences are partly explained by the general structural arrangement of bone tissue varying from widely flared ends and thin cortices to narrower mid-diaphyses with relatively thicker cortices.

From these results, it is apparent that BW provides a relatively poor standardization for locational differences in Ca in the lower limb, and that BMC/BW values cannot be assumed to reflect differences in bone mineral "density" at different locations. Locational differences in mean BMC/BW values (0.081 to 1.31 g/cm^2, mean 1.098 g/cm^2, coefficient of variation 5.1%) are more than twice those of BMC/CA (1.00 to 1.21 g/cm^3, mean 1.073 g/cm^3, coefficient of variation 2.4%). Age changes in these parameters are shown in Figure 15. In both males and females, BMC reaches a peak in the fourth decade, then declines, much more rapidly in females. Age changes in CA are similar, following patterns almost parallel to those in BMC. Age changes in BW follow a contrasting pattern, continuously increasing throughout adulthood. The increase in BW is greater among females at the femoral midshaft location illustrated here. The effects on age analyses of dividing BMC by BW and CA are shown in Figure 16. Age changes in BMC/BW are fairly similar to those observed in BMC, with the values for males declining only slightly in the three age groups and those for females declining much more rapidly. Thus, if BW is used to standardize BMC for bone volume differences, a significant decline with age in mineral "density" for females ($F = 0.47$, $p < 0.05$) is indicated. However, as shown in Figure 16, BMC standardized for true cortical area shows no significant age trend in either sex. The almost constant BMC/CA ratio indicates that the true mineral density at the femoral midshaft changes very little throughout adulthood.

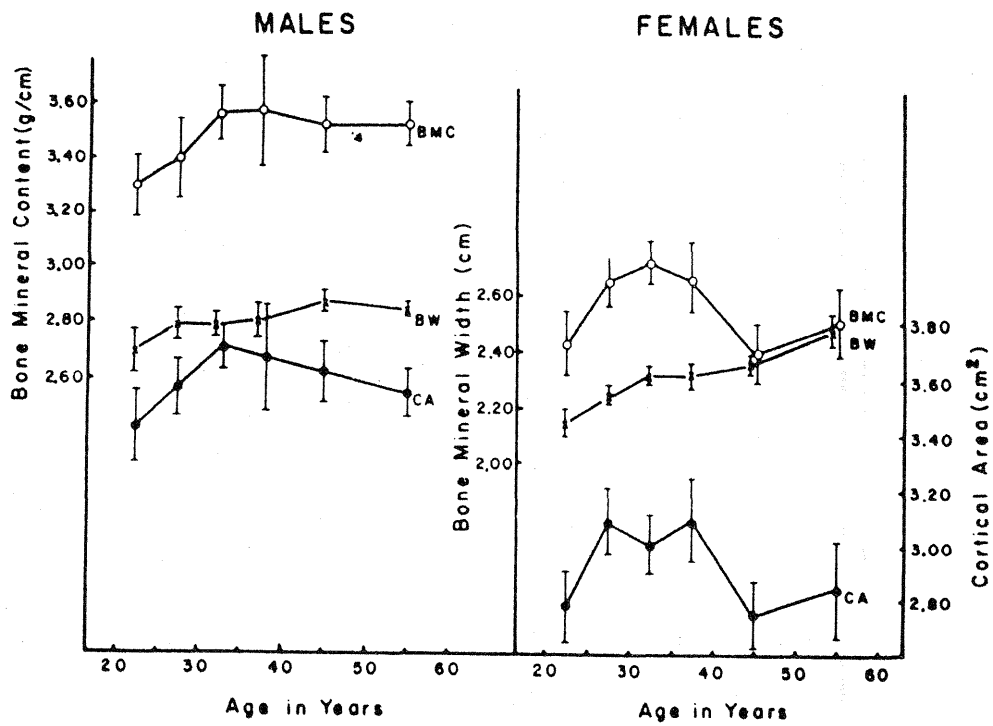

Figure 15. Changes with age in bone mineral content (BMC), bone width (BW), and cortical area (CA) at the femoral mid-shaft for the Pecos Pueblo population. Age changes in BMC are parallel to those in CA but not to those in BW. From (31); used with permission.

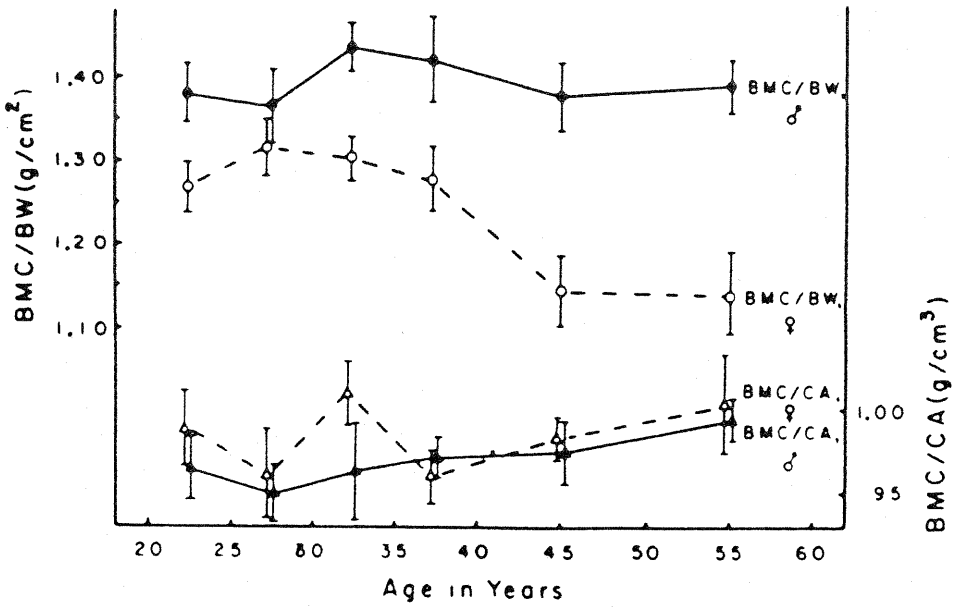

Figure 16. Changes with age in bone mineral content (BMC) normalized by bone width (BMC/BW) and by cortical area (BMC/CA) at the femoral mid-shaft for the Pecos Pueblo population. The BMC/BW ratio shows a significant decline with age in females but not in males. The BMC/CA ratio is constant throughout adulthood for both sexes, indicating no significant change in true mineral density at the femoral mid-shaft. From (31); used with permission.

We can conclude that variations in cortical bone area largely account for the variation in BMC between different locations in the lower limb, between males and females and between different age groups. We find no evidence for any significant sex or age differences in BMC standardized for true cortical area. Bone width also provides a poor estimate of bone volume differences in the lower limb. Variations in relative position of the endosteal boundary and cross-sectional shape are not reflected in a subperiosteal breadth measurement. As a consequence, standardizing BMC by BW can produce misleading results in locational, sex, and age comparisons. In particular, reductions with age in BMC/BW do not indicate reduced mineral density, but rather reduced cortical area relative to cortical subperiosteal area. Thus, age changes in bone mineral are mainly volumetric, not densitometric, at least through the seventh decade. Bone geometric remodeling appears to be an important part of the skeletal aging process. Variations in the types of remodeling which occur may be a significant factor in predisposing individuals to fracture in old age.

c) Consequences for diaphyseal fracture risk

These age-related geometric changes in long bone may also be viewed as a "compensatory" response to the reductions in material properties that occur with age (36). The data (Figure 9) indicate that the tensile strength of femoral cortical bone decreases by about 2% per decade in the age range 20 to 90. It is of interest to determine if the geometric changes shown in Figures 12 and 13 tend to compensate for this decrease by remodeling the

cross-section to a more efficient geometry. To explore this hypothesis, the eccentric axial loading analysis (similar to that illustrated in Figure 5 and described in Equation 3) can be applied to these data. The geometric data at the femoral mid-shaft for cortical area, moments of inertia, and eccentricity of the Pecos population are first substituted into a formulation similar to that of Equation 3. Using values for both young (20-39) and old (40+) segments of this population results in a predicted increase in the resistance to bending failure at the femoral mid-shaft of 6% for females and 8% for males. This increase is due primarily to the age-related increases in moments of inertia associated with the expanding periosteal and endosteal surfaces. The data in Figure 9 indicate a reduction of about 8% in the tensile strength of cortical bone in individuals in the same age groups. The nearly exact compensation for the reduced mechanical properties is striking.

These calculations are based on a number of simplifying assumptions. It should be noted that only longitudinal axial loads were considered, and that strength data from a modern sample were used for analyzing age-related geometric changes in the Pecos population. However, the observed changes in bone geometry are sufficient to suggest a kind of biomechanical homeostatic mechanism for maintaining long bones at approximately constant strength throughout adult life. This hypothesis certainly is worth examining further using more rigorous analytic methods and geometric data from both modern and ancient populations.

2. Prediction of vertebral fracture risk

Bone fracture represents the overriding clinical consequence of osteoporosis. Despite this, the biomechanical aspects of the disease have received little attention and the available clinical tools have not been shown to predict the risk of fracture reliably. To provide a practical example for the application of the biomechanical principles discussed in this chapter, we present some recent results from our laboratory (47) relative to predicting vertebral fracture risk using computed tomography. Our objectives with this investigation are to establish the accuracy of computed tomography as a measure of vertebral trabecular bone apparent density and to determine whether noninvasive techniques can be used to identify vertebrae "at risk" for the development of spontaneous fractures.

Twelve intact human lumbar spines (T11-L5) were harvested within 12 hours of death (age 63-99, mean age 78). Documentation on age, sex, cause of death and recent medical history was obtained and specimens were discarded if there was a history of back pain, spinal surgery, metastatic cancer or diseases affecting bone mineralization. Lumbar vertebrae L1 and L3 were designated as target vertebrae so that the endplates and discs immediately above and below these vertebrae could be incorporated in the mechanical testing procedures. A total of 16 vertebrae were suitable for analysis. The spines were doubly wrapped in plastic and frozen at -20° C until testing.

Computed tomographic scans were obtained using a General Electric 8800 scanner with the spine immersed in a water bath to improve CT resolution and avoid scatter. A phantom with chambers filled with water, ethyl alcohol and known concentrations of dipotassium hydrogen phosphate (K_2HPO_4) (5, 10, 20, 30 gm percent) was used to calibrate and monitor the accuracy of the scanner (24). The phantom and spine were positioned so that each scan "slice" included all chambers of the phantom. A computerized roentgenogram was used to center the first scan inferior to the superior endplate of each vertebra, with care being taken to exclude the endplate from the scan. Contiguous 5 mm scans (3-4/vertebra) were done, proximal-

to-distal, until the inferior endplate was reached. For each scan, CT values (Hounsfield units) were obtained from each chamber of the phantom, and from 6 pre-selected locations within the vertebral body. An average CT value for the interior trabecular bone was determined by using the cursor to outline a central region, positioned two pixels from the vertebral cortex and from the entrance of the basivertebral veins. Using a linear regression of the CT values for water and the solutions for K_2HPO_4, a corrected CT value for each measurement was then calculated (24).

For mechanical testing, each target vertebra was removed together with the proximal and distal endplates and discs. The posterior elements were removed by division of the pedicles. The endplates above and below the target vertebra were embedded in a test rig so that load was applied perpendicular to the endplates. Uniaxial compressive loads were applied using an electrohydraulic materials testing machine at a constant deformation rate of 0.01 mm/sec. Testing was discontinued immediately when there was an abrupt change in the slope of the load deformation curve with a loss of load-bearing capacity. After testing, the discs were removed and the endplates of the target vertebra examined for fracture. All dimensions of the vertebra were checked using a vernier caliper. After removal of the endplates, the vertebral body was machined under continuous irrigation to form 6 cylinders of trabecular bone. The cylinders measured 9.5 mm in diameter and 10-18 mm in height and were comprised of the trabecular bone from which

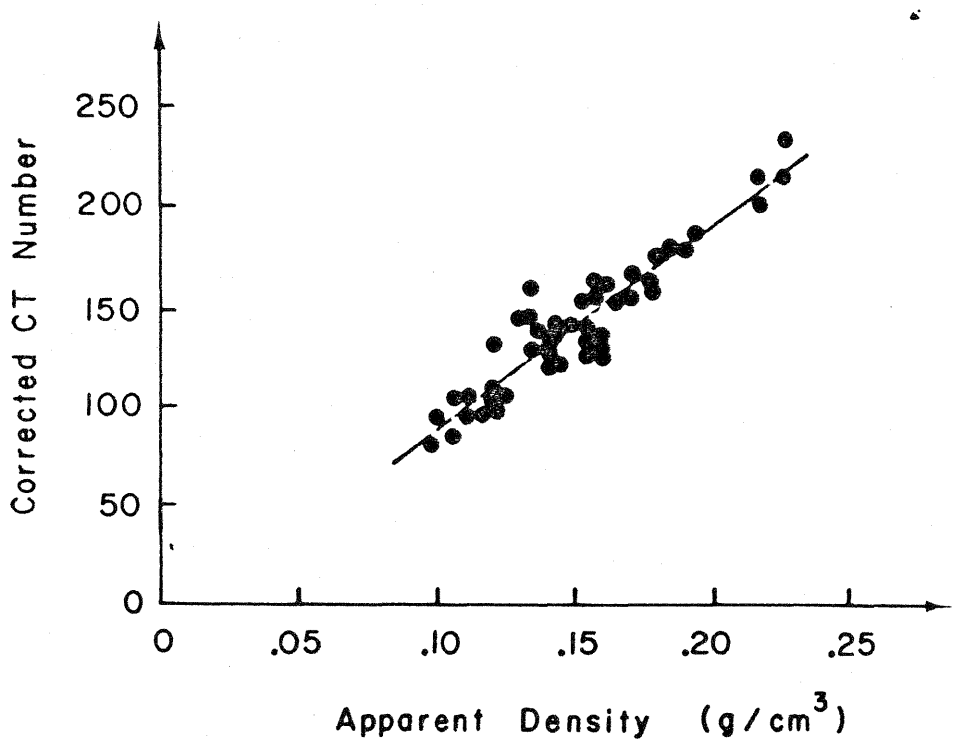

Figure 17. Correlation between calibrated CT number and apparent density of vertebral trabecular bone plugs ($R^2 = 0.89$, $P < 0.0001$). From (47); used with permission.

CT values had previously been determined. Hydrated weights of these specimens were calculated on an analytical balance and apparent density was calculated using standard methods (44,45).

a) Vertebral fracture risk

Computed tomography provided a very accurate quantitative measurement of bone apparent density. Once the CT values were corrected in terms of the reference calibration scale, there was a highly significant positive correlation ($R^2 = 0.89$; $p < 0.001$) between apparent density and corrected CT number (Figure 17). These calibration procedures were found to be essential, however. Despite frequent internal calibrations of the scanner so that the CT value of water was set at 0, we found variations from scan to scan of up to 10 H units for the density of water. This correlation of corrected CT value to apparent density did not vary between spines or between individual vertebrae. The vertebral failure load was taken to be the maximum load applied prior to the abrupt change in slope of the load-deformation curve. All target vertebrae failed by endplate fracture (9 superior and 7 inferior endplates). There was no visible disruption of the trabecular bone within the vertebral body which would affect apparent density measurements.

We showed (44,45) and discussed in previous sections that the compressive strength of trabecular bone is proportional to the apparent density squared. The most important determinants of the strength of trabecular bone are thus its apparent density and its cross-sectional area. Plotting vertebral failure load against the average apparent density squared multiplied by the cross-sectional area (Figure 18) resulted in highly significant correlations

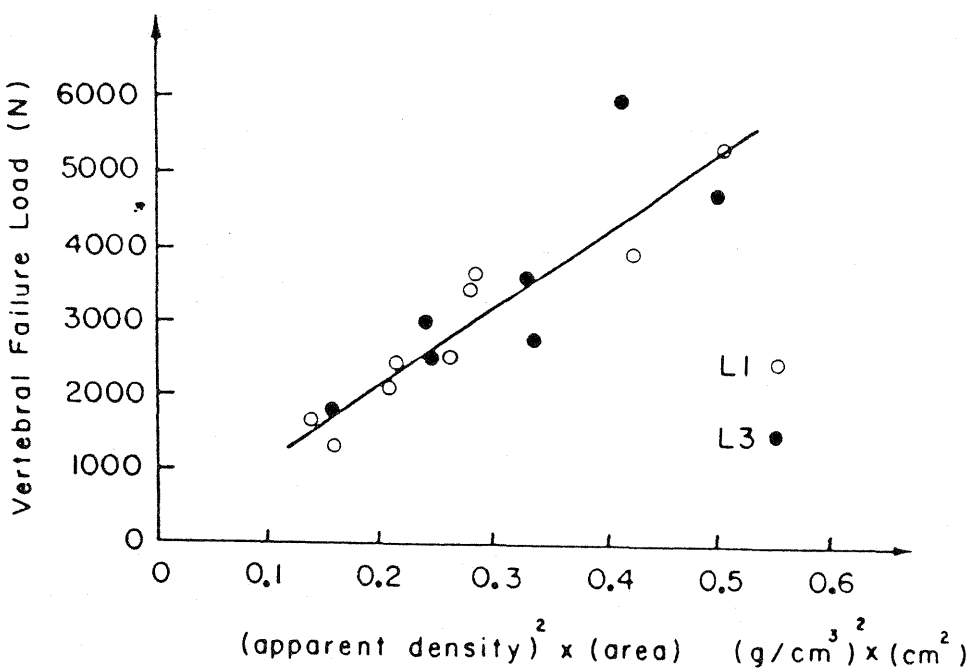

Figure 18. Correlation between vertebral failure load and average apparent density squared multiplied by cross-sectional area of trabecular bone within the vertebral body ($R^2 = 0.81$, $p < 0.0001$) From (47); used with permission).

(R^2 = 0.81, $p < 0.001$). This indicates that noninvasive determinations of vertebral density and cross-sectional area can be used with precision to predict vertebral failure load under these test conditions. The results thus suggest a simple but reliable noninvasive method for predicting vertebral fracture risk in vivo. With appropriate calibration procedures, the corrected CT numbers provide an accurate determination of vertebral trabecular apparent density. Moreover, a single regression equation adequately relates corrected CT number and apparent density for all vertebral bodies studied. Marrow fat content does not appear to vary significantly and thereby to affect this relationship. Hence, it may be possible to apply this approach without having to resort to dual energy CT measurements.

Surprisingly, the relationship between vertebral failure load and the noninvasive determinations of trabecular density and area was relatively simple, indicating that axial compressive stresses in the interior trabecular bone are an important feature of vertebral loading. We thus do not have to resort to more sophisticated models to represent the relative contributions of cortical and trabecular bone, as might be assumed from previous studies (22,48-51). This may be a consequence of our use of more physiologic load transmission through disc and endplate to perform failure tests. It remains to be determined from retrospective or prospective clinical studies whether this simple model will provide a useful tool for identifying individual patients at increased risk for spontaneous vertebral fracture. These findings would also suggest that, under these loading conditions, the thin shell surrounding the trabecular bone in the vertebral centrum makes only a modest contribution to the structural strength of the vertebral body.

b) Structural contributions of vertebral cortical shell

The relative contributions of trabecular bone and the cortical shell to the load-bearing capacity of the vertebra has been the subject of much controversy (37,49,51,52). In the most recent of these studies, Rockoff et al (51) reported that the cortex contributes 45-75% to the peak strength of the vertebral body under compressive loading. Given the limitations of the measurements of the cortical shell by CT, this would suggest possible difficulties in relating QCT (quantitative CT) to vertebral strength. Several earlier studies, however, suggested that the contribution of the central trabecular region is more significant than that of the cortical shell (49,52). To address this issue, we also conducted additional experiments to assess the structural contributions of the vertebral cortical shell.

The relative contribution of the cortical shell and trabecular bone to the strength of the vertebral body was assessed using 40 L1 and L3 vertebrae, 20 from the above experiments and 20 additional vertebrae excised from 10 additional spines. The 40 vertebrae were divided into two groups of L1, L3 specimen pairs. To determine if the compressive failure loads for L1 and L3 from the same spine were similar, the first and third lumbar vertebrae from 10 spines were prepared, mounted and mechanically tested as described above. The entire cortex of the L1 specimens from the remaining 10 spines was removed by painstaking manual sanding, with frequent water picking to prevent inadvertant damage to the underlying trabecular bone. Attempted removal of the cortex using power instruments invariably destroyed some of the trabecular bone and created localized stress concentrations. The importance of the cortex to the vertebral body was assessed by comparing the difference in strength of L1 and L3 for the 10 spines with the cortex intact with the difference in strength of L1 and L3 for the 10 spines from which the cortex of L1 had been removed.

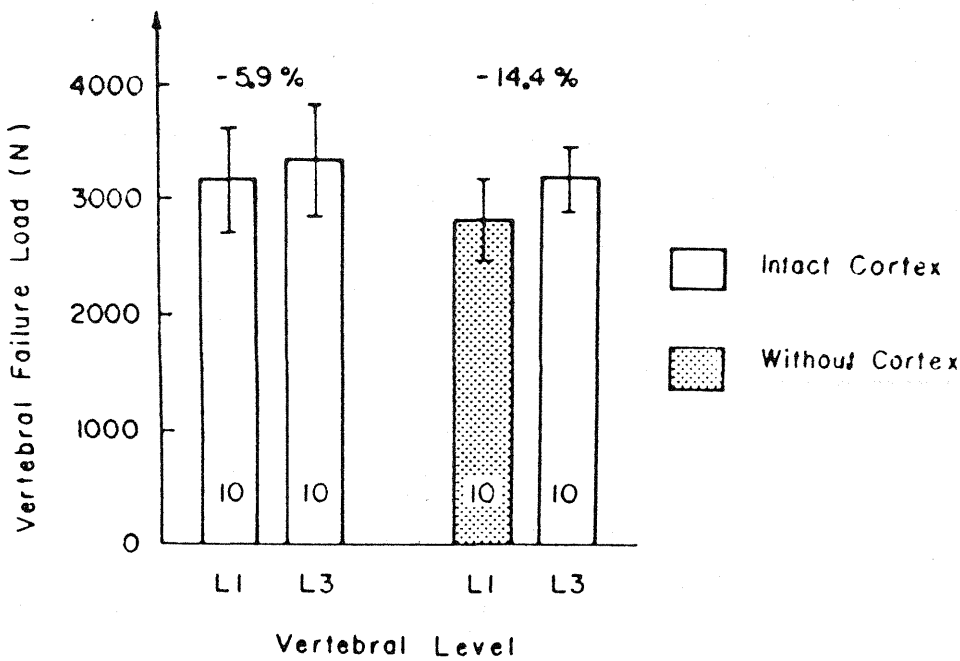

Figure 19. Reductions in load-bearing capacity of lumbar vertebrae due to removal of cortical shell. On left, average failure loads of 10 spines with L1 and L3 cortices intact ($p > 0.05$). On right, failure loads of 10 spines in which L1 cortex had been removed and the L3 cortex maintained intact (significant difference, $p < 0.05$). The modest reduction in strength due to removal of the cortex is far less than the 40-75% values reported in the literature. From (47); used with permission).

The cortical shell was found to contribute very little to the overall strength of the vertebral body (Figure 19). For vertebral bodies tested intact, the average failure load for L1 was 3160 N (n = 10, 95% C.I. = 891 N) and for L3, 3385 N (n = 10, 95% C.I. = 995 N). Thus, with the vertebral cortex intact, the average failure load of L1 was 5.86% less than that of L3 (n = 10, 95% C.I. = 4.9%). In the 10 additional spines, for L1 vertebrae tested without cortex, the average failure load was 2771 N (n = 10, 95% C.I. = 737 N). For these 10 spines, the average failure load for L3 vertebral bodies was again determined with the cortex intact and found to be 3176 N (n = 10, 95% C.I. = 618 N). The two groups of intact L3 vertebrae were found not to be significantly different ($P > .05$), indicating that the two groups of vertebral specimens could be assumed to be from the same population. In the second set of 10 spines, the mean percent difference in strength between L3 and L1 (without cortex) was 14.4% (n = 10, 95% C.I. = 11.4). When this percent difference is compared by unpaired t-test with the percent difference in strength of L1 and L3 for the 10 spines with an intact L1 cortex, this difference is significant ($p < 0.05$).

The observed reduction in strength is much less than the 40-75% reduction reported by Rockoff et al (51). This may be a consequence of different methodologies used in preparation and testing. The vertebral bodies used in the study of Rockoff et al were soaked in ethanol prior to testing and

this may have altered the failure properties of the trabecular bone. The peak load in their study was estimated to occur at the first sign of deviation from non-linearity of the steepest slope of the load-deformation curve. Our load deformation curves showed that peak loads as determined by the criteria of Rockoff et al had a variable relationship to our vertebral failure load. In addition, in our hands, removal of the cortical shell using a high-speed circular hand saw (as reported by Rockoff et al) invariably damaged the underlying trabecular bone and caused localized stress concentrations which may have influenced the earlier conclusions. Our results indicate that, when subjected to uniaxial compression at a slow deformation rate, the cortex of the lumbar vertebrae contributes little to the yield strength of the vertebral body. Thus, one of the advantages claimed for spinal dual photon absorptiometry (DPA) (i.e., that it provides an integrated measure of both cortical and trabecular contributions to mineral content) does not seem to be significant based on the relative biomechanical contributions of these regions. Instead it appears to be sufficient to distinguish between cortical and trabecular components and then to determine the apparent density and compressive strength of the central trabecular bone. Using the simple relationships established here, QCT measurements seem to be well-suited for this purpose. Note also that the limited structural role played by the vertebral cortical shell in these studies is consistent with the direct measurements of the strength and stiffness of the metaphyseal shell (Table 3).

In summary, our results show that, with appropriate calibration, single energy quantitative computed tomography can be used to predict the local apparent density of trabecular bone. The presence of variable fat content does not appear to compromise this relationship significantly. The average apparent density of the interior trabecular bone can be used to predict the failure load of vertebral bodies with posterior elements removed in response to uniaxial compressive loads. Multiplying the squared apparent density of the vertebral trabecular bone by the area ($\rho^2 A$) provides a highly significant predictor of vertebral failure load ($R^2 = 0.81$, $p < .0001$) under these in vitro test conditions. It remains to be demonstrated from retrospective or prospective clinical studies whether this simple parameter will provide a useful tool for identifying individual patients at increased risk for spontaneous vertebral fractures.

E. SUMMARY

We have shown in this review that the structural behavior of bone can be approached on two levels: a material level and a structural level. The material level is investigated by preparing specimens of regular geometry and determining their mechanical properties. In this step, the effects of complex bone geometries are eliminated by normalizing for cross-sectional area and length. Structural behavior, on the other hand, includes contributions both from the mechanical properties (at the material level) and the effects of complex bone geometries. These basic concepts were summarized and the loading patterns to be expected to be in whole bones briefly reviewed. An important point is that long bones behave as slightly curved beams subjected to axial, compressive loads applied at the bone ends. This situation is similar to the axial, compressive loading of slightly curved beams and thus results in reduced tensile stresses on the convex surface and increased compressive stresses on the concave surface of a bone. It is thought that this loading situation is an attempt to compensate for the differences in compressive and tensile strengths of cortical bone.

With this introduction, the mechanical properties of bone tissue were summarized, emphasizing first the viscoelastic and anisotropic characteristics of cortical bone. For trabecular bone, the most important feature controlling mechanical properties is the apparent density. Strength is related to the square of the apparent density and modulus to the cube of the apparent density. These power law relations hold for all bone throughout the skeleton and indicate the remarkable sensitivity of bone to changes in porosity. Direct measures of the mechanical properties of the metaphyseal shell were also reported. These indicate that the structural contribution of these metaphyseal regions is far less than has been commonly assumed.

Two examples were used to indicate how the geometric characteristics and material properties in bone combine to determine the structural behavior of whole bones. The first example relied on data describing geometric changes with age in a large population sample from the Pecos Pueblo Indians. These studies indicate that aging results in both subperiosteal and endosteal expansion. This in turn produces an increase in the moment of inertia, resulting in a cross-sectional shape which is more efficient for resisting bending and torsion. Unfortunately, these age-related geometric changes tend to confound the use of bone width measures as a normalization factor for photon absorptiometry. Bone width measurements do not in general correspond to the actual changes in cortical area with age and thus previous assumptions on changes in bone mineral content with age may need to be re-examined. It is also of interest to note that these geometric changes tend to compensate for the reductions in bone material properties that occur with age. These biomechanical compensatory mechanisms suggest a kind of homeostatic mechanism which may be active in bone. The nearly exact agreement between the predicted increases in bending resistance at the femoral midshaft and the measured reductions in tensile strength of bone is an intriguing finding and deserves further study using more exact analytical techniques, improved information on loading, and further geometric studies of modern populations.

Finally, we showed applications of these techniques to the development of noninvasive, biomechanical predictors of fracture risk in vertebral bodies. The results suggest that quantitative computed tomographic scans can be used with suitable precision to predict the apparent density of trabecular bone in the vertebral centrum. These predictions can in turn be used to estimate the compressive strength of trabecular bone and thereby to predict failure loads for the vertebral body. The strong agreement between the predicted failure loads and those actually measured suggests that these methods can be used to develop noninvasive predictors of fracture risk *in vivo*. The results also suggest that the structural contribution of the vertebral cortical shell is far less than has been previously assumed. This finding is in apparent agreement with our direct measurements of the metaphyseal shell.

Future research directions. These examples suggest an emerging possibility in the field of musculoskeletal biomechanics—the ability to predict (and therefore assess) the *in vivo* structural capacity of regions of the skeleton. Only two relatively *simple* examples were discussed here. These were axial loading of long bones and direct compressive loading of vertebral bodies. In both instances, however, using available data on mechanical properties of bone tissues and on the geometries of the involved regions, simple biomechanical analyses could be used to predict a number of aspects of *in vivo* structural behavior. In one instance these analyses produced information on compensatory remodeling of long bone cross-sections with age. The geometric data also provide baseline information of importance to the proper interpretation of photon absorptiometric scans.

In the second instance, such biomechanical analyses could be used to develop CT-based, noninvasive procedures for predicting fracture risk in the vertebral body. While only simplified loading situations were used, the predictive capabilities of these analyses were sufficiently precise to suggest both testing these predictors in clinical settings and extending the approach to other vertebral modes.

There are several obvious extensions of the preliminary approaches outlined here. For the structural behavior of long bones, it is clearly of interest to extend the availability of geometric databases from the archaeological populations considered herein to similar samples from modern populations. Such modern data would provide an opportunity to compare the effects of physical activity and other cultural influences on the geometry of long bones. Combined with the expanding information on in vivo loading of long bones, such databases could be used (along with more refined analytic techniques) to explore the physical parameters governing the age-related remodeling of long bones. The hypothesis suggested by our simple analysis is that long bones remodel with age in order to maintain a bone of approximately constant bending strength. This hypothesis could be tested rigorously in modern populations using refined methods for stress distributions in beams of complex cross-section. The actual prediction of fracture risk in long bones of the axial skeleton based on CT scans in individual patients would then be a distinct possibility.

It would also be of great interest to extend these analytical predictors to skeletal regions such as the proximal femur for which an increased fracture risk is observed clinically and is of particularly dire consequences to the patient. The geometric, material, and loading complexities of such regions, however, require that even more sophisticated analytical techniques (such as the finite element method) be used for stress prediction. Such analytical techniques are now available. These methods, coupled with improved experimental data on the material properties of metaphyseal bone in the proximal femur, and CT scans to determine local geometries, could be used to provide accurate predictors of fracture risk in individual patients. The value of such predictors would be of obvious significance in guiding the assessment and treatment of osteoporosis.

References

1. Hayes, W.C. and Snyder, B.D. (1981): Toward a quantitative formulation of Wolff's law in trabecular bone. In: Symposium on the Mechanical Properties of Bone, pp. 43-68. American Society of Mechanical Engineers, Boulder, Colorado.
2. Woo, S.L.-Y., Kuei, S.C., Amiel, D., Hayes, W.C., White, F.C., and Akeson, W.H. (1981): The effect of prolonged physical training on the properties of long bone. Journal of Bone and Joint Surgery, 63A: 780-786.
3. Jowsey, J (1977). In: Metabolic Diseases of Bone. W.B. Saunders, Philadelphia.
4. Lane, J.M. and Vigorita, V.J. (1983): Osteoporosis: current concepts review. Journal of Bone and Joint Surgery, 65A:274-278.
5. Hayes, W.C. (1979): Biomechanics of fracture treatment. In: Fracture Healing and Treatment, pp. 124-172. Editor: R.B. Heppenstall. W.B. Saunders, Philadelphia.
6. Avioli, L.V. (editor) (1983): The Osteoporotic Syndrome: Detection, Prevention, and Treatment. Grune and Stratton, New York.

7. Kelsey, J.L., Pastides, H., and Bisbee, G.E., Jr. (1978): Musculoskeletal Disorders: Their Frequency of Occurrence and Their Impact on the Population of the United States. Prodist, New York.
8. Recker, R.R. (editor) (1983): Bone Histomorphometry: Techniques and Interpretation. CRC Press, Boca Raton, Florida.
9. Cohn, S.H. (editor) (1981): Non-invasive Measurements of Bone Mass and Their Clinical Application. CRC Press, Boca Raton, Florida.
10. Dequeker, J. and Johnston, C.C., Jr. (1982): In: Non-invasive Measurements: Histological Problems. Radiogrammetry, Single and Dual Photon Absorptiometry, Neutron Activation and C.T. Densitometry. IRL Press, Washington, D.C.
11. Mazess, R.B. (1983): Noninvasive methods for quantitating trabecular bone. In: The Osteoporotic Syndrome: Detection, Prevention, and Treatment, pp. 85-114. Editor: L.V. Avioli. Grune and Stratton, New York.
12. Mazess, R.B. (1983): The non-invasive measurement of skeletal mass. In: Bone and Mineral Research, Annual II, pp. 223-279. Editor: W.A. Peck. Elsevier, Amsterdam.
13. Singh, M., Riggs, L., Beabout, J.W., and Jowsey, J. (1972): Femoral trabecular pattern index for evaluation of spinal osteoporosis. Annals of Internal Medicine, 77:63-67.
14. Meema, H.E. and Meema, S. (1981): Radiogrammetry. In: Non-invasive Measurements of Bone Mass and Their Clinical Applications, pp. 5-50. Editor: S.H. Cohn. CRC Press, Boca Raton, Florida.
15. Colbert, C. and Bachtell, R.S. (1981): Radiographic absorptiometry (photodensitometry). In: Non-invasive Measurements of Bone Mass and Their Clinical Application. Editor: S.H. Cohn. CRC Press, Boca Raton, Florida.
16. Ruff, C.B. and Hayes, W.C. (1982): Subperiosteal expansion and cortical remodeling of the human femur and tibia with aging. Science, 217:945-948.
17. Ruff, C.B. and Hayes, W.C. (1983): Cross-sectional geometry of Pecos Pueblo femora and tibiae: a biomechanical investigation. I. Method and general patterns of variation. American Journal of Physical Anthropology, 60:359-381.
18. Ruff, C.B. and Hayes, W.C. (1983): Cross-sectional geometry of Pecos Pueblo femora and tibiae: a biomechanical investigation. II. Sex, age and side differences. American Journal of Physical Anthropology, 60:383-400.
19. Mazess, R.B., Peppler, W.W., Chestnut, C.H., III, Nelp, W.B., Cohn, S.H., and Zanzi, I. (1981): Total body bone mineral and lean body mass by dual-photon absorptiometry. II. Comparison with total body calcium by neutron activation analysis. Calcified Tissue International, 33:361-362.
20. Mazess, R.B., Peppler, W.W., Harrison, J.E., and McNeill, K.G. (1981): Total body bone mineral and lean body mass by dual-photon absorptiometry. III. Comparison with trunk calcium by neutron activation analysis. Calcified Tissue International, 33:365-368.
21. Peppler, W.W. and Mazess, R.B. (1981): Total body bone mineral and lean body mass by dual-photon absorptiometry. I. Theory and measurement procedure. Calcified Tissue International, 33:353-359.
22. Bradley, J.G., Huang, H.K., and Ledley, R.S. (1978): Evaluation of calcium in bones from CT scans. Radiology, 128:103-107, 1978.
23. Genant, H.K. and Boyd, D. (1977): Quantitative bone mineral analysis using dual energy computed tomography. Investigative Radiology, 12:545-551.

24. Genant, H.K., Boyd, D., Rosenfeld, D., Abols, Y., and Cann, C.E. (1981): Computed tomography. In: Non-invasive Measurement of Bone Mass and Their Clinical Application, pp. 121-149. Editor: S.H. Cohen. CRC Press, Boca Raton, Florida.
25. Posner, I. and Griffiths, H.J. (1977): Comparison of CT scanning with photon absorptiometric measurements of bone mineral content in the appendicular skeleton. Investigative Radiology, 12:542-544.
26. Reich, N.E., Seidelmann, F.E., and Tubbs, R.R. (1976): Determination of bone mineral content using CT scanning. American Journal of Roentgenology, 127:593-594.
27. Ruegsegger, P., Dambacher, M.A., Ruegsegger, E., Fischer, J.A., and Anliker, M. (1984): Bone loss in premenopausal and postmenopausal women. Journal of Bone and Joint Surgery, 66A:1015-1023.
28. Ruegsegger, R., Elsasser, V., and Anliker, M. (1976): Quantification of bone mineralization using computed tomography. Radiology, 121:93-97.
29. Reilly, D.T. and Burstein, A.H. (1974): The mechanical properties of cortical bone. Journal of Bone and Joint Surgery, 56A: 1001-1022.
30. Reilly, D.T., Burstein, A.H., and Frankel, V.H. (1974): The elastic modulus for bone. Journal of Biomechanics, 7:271-275.
31. Ruff, C.B. and Hayes, W.C. (1984): Bone mineral content in the lower limb: relationship to cross-sectional geometry. Journal of Bone and Joint Surgery, 66A:1024-1031.
32. Nagurka, M.L. and Hayes, W.C. (1980): Technical note: an interactive graphics package for calculating cross-sectional properties of complex shapes. Journal of Biomechanics, 13:59-64.
33. Burstein, A.H., Currey, J.D., Frankel, V.H., and Reilly, D.T. (1972): The ultimate properties of bone tissue: the effects of yielding. Journal of Biomechanics, 5:35-44.
34. Burstein, A.H., Currey, J., Frankel, V.H., Heiple, K.G., Linseth, P., and Vessely, J.C. (1972): Bone strength: the effect of screw holes. Journal of Bone and Joint Surgery, 54A:1143-1156.
35. Burstein, A.H., Zika, J.M., Heiple, K.G., and Klein, L. (1975): Contribution of collagen and mineral to the elastic-plastic properties of bone. Journal of Bone and Joint Surgery, 57:956-961.
36. Burstein, A.H., Reilly, D.T., and Martens, M. (1976): Aging of bone tissue: mechanical properties. Journal of Bone and Joint Surgery, 58A: 82-86.
37. Evans, F.G. (1957): Stress and Strain in Bones. Charles C. Thomas, Springfield, Illinois.
38. Evans, F.G. (1973): Mechanical Properties of Bone. Charles C. Thomas, Springfield, Illinois.
39. Hayes, W.C. (1978): Biomechanical measurements of bone. In: CRC Handbook of Engineering in Medicine and Biology. Section B. Instruments and Measurements, Volume 1, pp. 333-372. Editor: E. Bahniuk. CRC Press, Cleveland, Ohio.
40. Hayes, W.C. and Carter, D.R. (1979): Biomechanics of bone. In: Skeletal Research: An Experimental Approach, pp. 263-300. Editor: A.S. Kunin. Academic Press, New York.
41. Wright, T.M. and Hayes, W.C. (1976): Tensile testing of bone over a wide range of strain rates. Effects of strain rate, microstructure and density. Medical and Biological Engineering, 14:671-680.
42. Wright, T.M. (1980): Mechanics of fracture and fracture propagation. In: Scientific Foundations of Orthopaedics, pp. 252-258. Editor: P. Bullough. William Heinemann Medical Books, London.

43. Carter, D.R. and Spengler, D.M. (1978): Mechanical properties and composition of cortical bone. Clinical Orthopaedics, 135:192-217.
44. Carter, D.R. and Hayes, W.C. (1976): Bone compressive strength: the influence of density and strain rate. Science, 194:1174-1176.
45. Carter, D.R. and Hayes, W.C. (1977): The compressive behavior of bone as a two-phase porous structure. Journal of Bone and Joint Surgery, 59A:954-962.
46. Carter, D.R. Schwab, G.H., and Spangler, D.M. (1980): Tensile fracture of cancellous bone. Acta Orthopaedica Scandinavica, 51:733-741.
47. McBroom, R.J., Hayes, W.C., Edwards, W.T., Goldberg, R.P., and White, A.A. (in press): Prediction of vertebral body compressive fracture using quantitative computed tomography. Journal of Bone and Joint Surgery.
48. Atkinson, P.J. (1966): Variation in trabecular structure of the vertebrae with age. Calcified Tissue Research, 1:24-32.
49. Bell, G.H., Dunbar, O., and Beck, J.S. (1967): Variations in strength of vertebrae with age and their relation to osteoporosis. Calcified Tissue Research, 1:75-86.
50. Kazarian, L.E. and Graves, G.A. (1977): Compressive strength characteristics of the human vertebral centrum. Spine, 2:1-14.
51. Rockoff, S.D., Sweet, E., and Bleustein, J. (1969): The relative contribution of trabecular and cortical bone to the strength of human lumbar vertebrae. Calcified Tissue Research, 3:163-175.
52. Bartley, M.H., Arnold, J.S., Haslam, R.K., and Jee, W.S.S. (1966): The relationship of bone strength and bone quantity in health, disease and aging. Journal of Gerontology, 21:517-521.
53. Reilly, D.T. and Burstein, A.H. (1975): The elastic and ultimate properties of compact bone tissue. Journal of Biomechanics, 8:393-405.
54. Murray, R.P., Hayes, W.C., Edwards, W.T., and Harry, J.D. (1984): Mechanical properties of the subchondral plate and the metaphyseal shell. In: Transactions, 30th Annual Meeting, Orthopedic Research Society.